Energy Advances

ROYAL SOCIETY OF CHEMISTRY

PAPER

View Article Online
View Journal | View Issue

Cite this: *Energy Adv.*, 2023, 2, 530

Structure and interactions of novel ether-functionalised morpholinium and piperidinium ionic liquids with lithium salts†

Anna Warrington, [ac] Luke A. O'Dell, [b] Oliver E. Hutt, [c] Maria Forsyth [a] and Jennifer M. Pringle *[a]

Received 9th December 2022,
Accepted 27th February 2023

DOI: 10.1039/d2ya00348a

rsc.li/energy-advances

Ionic liquids with ether-functionalised cations have generated much interest as electrolytes for Li-ion batteries because of their intrinsic safety properties such as non-flammability, in addition to the advantageous fluidity and lithium coordination environment afforded by the ether group. Here, four ionic liquids, *N*-methoxymethyl-*N*-piperidinium bis(fluorosulfonyl)imide and bis(trifluoromethanesulfonyl)imide ([C_{1O1}mpip][FSI] and [C_{1O1}mpip][TFSI]) and *N*-methoxymethyl-*N*-methylmorpholinium FSI and TFSI ([C_{1O1}mmor][FSI] and [C_{1O1}mmor][TFSI]) were synthesised and compared to explore the suitability of these ionic liquids as battery electrolytes. Properties fundamentally relevant to electrolyte applications, such as thermal stability, density, viscosity and ionic conductivity and electrochemical stability were analysed to evaluate the effects caused by the presence of ether-functionality in the side chain and/or in the organic cation ring. Electrolyte solutions were prepared with lithium bis(fluorosulfonyl)imide (LiFSI) or lithium bis(trifluoromethanesulfonyl)imide (LiTFSI) in a ratio of 1 : 9 salt : IL (mol/mol). The electrolyte solutions were found to exhibit glass transition temperatures between −64 and −94 °C. $(LiFSI)_{0.1}([C_{1O1}mpip][FSI])_{0.9}$ exhibited the highest ionic conductivity of 5.0×10^{-3} S cm^{-1} and fastest Li^+ diffusion of 1.6×10^{-11} m^2 s^{-1} at 30 °C. The TFSI-based ionic liquids and their electrolyte solutions were analysed with Raman spectroscopy and the [C_{1O1}mmor][TFSI] exhibited a lower average solvation number of Li^+ (1.49) than [C_{1O1}mpip][TFSI] (1.65) demonstrating the benefit of an oxygen in the ring.

Introduction

Advancements in lithium battery technologies require the development of innovative new materials to achieve higher performance in energy density, safety, and durability. For electrolytes, one approach to reach these goals is through the utilisation of alternative safer and more reliable electrolytes than flammable and volatile organic carbonates. Ionic liquids (ILs) are an appealing class of compounds to meet requirements of new aprotic solvents because of their intrinsic properties such as negligible flammability and volatility, high thermal stability, wide temperature range,[1] and wide electrochemical windows.[2]

ILs are liquid salts at room temperature, are formed with an organic cation commonly based on pyrrolidinium, piperidinium, morpholinium, ammonium, imidazolium, and an inorganic or organic anion *e.g.* PF_6^-, BF_4^-, dicyanamide, bis-(trifluoromethanesulfonyl)imide (TFSI), bis(fluorosulfonyl)imide (FSI). Among the various anions, fluorinated anions such as TFSI and FSI have been widely studied due to their wide electrochemical stability, low viscosity, and ability to form stable and conductive solid–electrolyte interface (SEI) layers.[3–8] Both lithium bis(trifluoromethanesulfonyl)imide (LiTFSI) and lithium bis(fluorosulfonyl)imide (LiFSI) are commercially available and considered suitable for battery applications.

One method to further reduce viscosity and enhance ionic conductivity is through the incorporation of ether functional groups on the cation.[9–12] For example, at 30 °C, the viscosity and ionic conductivity of the neat IL (without any lithium salt) 1-methoxymethyl-1,1,1-trimethylammonium TFSI [$N_{111,1O1}$][TFSI] is 44 mPa s and 4.8 mS cm^{-1}, compared to 63 mPa s and 3.5 mS cm^{-1} for the alkyl equivalent 1-propyl-1,1,1-trimethylammonium TFSI [N_{1113}][TFSI].[13,14] In another study, the viscosity and ionic conductivity of (*N*-(2-methoxyethoxy)methyl)-*N*-methylpiperidinium TFSI [$C_{(1O2O1)}$mpip][TFSI] at 30 °C is 69 mPa s and 2.3 mS cm^{-1} respectively, compared to 132 mPa s and 0.8 mS cm^{-1} for *N*-hexyl-*N*-methylpiperidinium TFSI [C_6mpip][TFSI].[15]

[a] *Institute for Frontier Materials, Deakin University, Burwood, VIC 3125, Australia. E-mail: jenny.pringle@deakin.edu.au*
[b] *Institute for Frontier Materials, Deakin University, Geelong, VIC 3216, Australia*
[c] *Boron Molecular, 500 Princes Hwy, Noble Park, VIC 3174, Australia*

† Electronic supplementary information (ESI) available: Additional TGA, density, viscosity, conductivity, PFG-NMR, Infrared and Raman spectroscopy, VTF fittings and cyclic voltammograms. See DOI: https://doi.org/10.1039/d2ya00348a

For lithium batteries, IL electrolytes are prepared by dissolving the corresponding lithium salt (*e.g.* LiTFSI) in an IL. Li^+ mobility remains a significant challenge in IL electrolytes as Li^+ ions usually diffuse slower than the cations and free anions in the IL, as they are coordinated to anions by strong electrostatic interactions, therefore Li^+ transport is highly dependent on the Li^+ solvate structures. In TFSI- and FSI-based ILs, Li^+ is coordinated to the oxygens in the anion, to form $[Li(anion)_n]^{1-n}$ complexes, where n is the average number of anions solvating one Li-ion.[16] In electrolyte solutions with low concentrations of Li-salt a high solvation number can be associated with limitations to Li-insertion in the negative electrode at low current densities, and Li-diffusion, directly impacting charge–discharge rates at high current densities.[17] Raman spectroscopy studies highlight the benefit of oxygen-functionality on the cation when paired with TFSI, FSI,[18] dicyanamide (DCA) and mixed anions.[19,20] The ether–oxygen is known to play a key role in weakening interactions between Li^+ and the anion, by providing a new speciation site for the Li^+ to interact with.[12,21] A lower solvation number of anions per Li^+ can therefore lead to better rate performance in batteries.

Understanding the factors that influence Li^+ solvation and transport is therefore necessary in the development of new electrolytes, especially how the oxygen in the chain *vs.* the ring can influence the solvation environment of Li^+ and lead to changes in anion solvation, which has not yet been studied. Furthermore, lower viscosity ionic liquid-based electrolytes are required to improve battery performance.

In the present study four ILs were newly synthesised, with two cations, *N*-methoxymethyl-*N*-piperidinium ($[C_{1O1}mpip]^+$) and *N*-methoxymethyl-*N*-methylmorpholinium ($[C_{1O1}mmor]^+$) paired with FSI and TFSI anions, shown in Fig. 1, as potential electrolytes for lithium batteries. The methoxymethyl chain has been less explored in comparison to longer ether-functionalised chains but has previously been employed on cations such as *N*-methoxymethyl-*N*-methylpyrrolidinium $[C_{1O1}mpyr]^+$ and 1-methoxymethyl-1,1,1-trimethylammonium $[N_{111,1O1}]^+$ to demonstrate the promising benefits of the chain.[13,22] $[N_{111,1O1}][TFSI]$ led to improved fluidity and lower ionicity compared to the alkyl equivalent IL, $[N_{1113}][TFSI]$, and longer ether-functionalised chains such as $[N_{111,2O1}][TFSI]$, but Li–electrolytes based on these ILs have not yet been studied. Further, the viscosity of $[C_{1O1}mpyr][FSI]$ at 25 °C is 31 mPa s, lower than most ILs, and 0.32 kg mol^{-1} LiFSI in $[C_{1O1}mpyr][FSI]$ has been used to demonstrate stable lithium plating and stripping with a higher current density than alkyl ILs.[23] $[C_{1O1}mpip][TFSI]$ has previously been synthesised at 27% yield, and an improved synthetic method is reported here. The IL was previously studied as an electrolyte for high temperature supercapacitor operation and outperformed the standard 1.0 M LiTFSI propylene carbonate electrolyte,[24] so a deeper understanding of the physicochemical properties of this IL is desirable.

Here we report the thermal transitions and decomposition temperatures of the ILs, and the transport properties of the neat ILs and their corresponding 10 mol% lithium electrolytes with the same anion. We investigated the influence of the two cation structures on Li–TFSI interactions using Fourier Transform Infrared and Raman spectroscopy to reveal insights into the different solvation environments of the lithium ions, which is important for the development of these materials as electrolytes for lithium batteries.

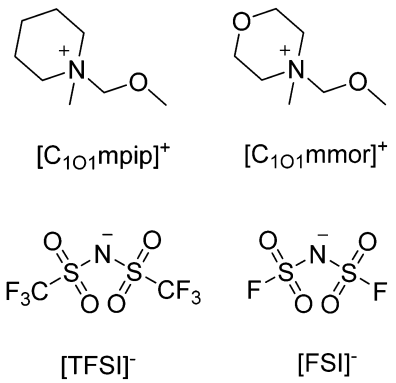

Fig. 1 Structure and abbreviations of cation and anions used. Cation abbreviations are: *N*-methoxymethyl-*N*-methylpiperidinium $[C_{1O1}mpip]^+$ and 4-methoxymethyl-4-methylmorpholinium $[C_{1O1}mmor]^+$. Anion abbreviations are bis(trifluoromethanesulfonyl)imide $[TFSI]^-$, and bis(fluorosulfonyl)imide $[FSI]^-$.

Experimental

Materials and methods

4-Methylmorpholine (Oakwood Chemicals, USA), *N*-methylpiperidine (Oakwood Chemicals, USA) were distilled before use. Lithium bis(trifluoromethanesulfonyl)imide (LiTFSI) (99.9%, Solvay, Canada), potassium bis(fluorosulfonyl)imide (KFSI) (99.9%, Suzhou Fluolyte Co, China), lithium bis(fluorosulfonyl)imide (99.9%, Solvay, Canada), were dried at 50 °C for at least 24 hours before use. Chloromethylmethyl ether (97%, Boron Molecular, Australia) and silver nitrate ($AgNO_3$) (LR, Chem-Supply, Australia) were used without further purification.

Liquid-state ^1H, ^{13}C and ^{19}F NMR spectra were collected on a 9.4 T Bruker Avance III instrument. Mass spectroscopy was performed on an Agilent 1200 series HPLC system. Elemental analysis was performed at Macquarie University Chemical Analysis Facility, Australia. After preparation of the ILs they were dried under vacuum at 60 °C for at least 72 hours after which they were transferred to an Ar-filled glove box for storage and handling.

Chloride content and Karl Fisher coulometric titration

Quantification of residual chloride content was not possible by ion selective electrode, due to interaction of the organic cations, $[C_{1O1}mpip]^+$ and $[C_{1O1}mmor]^+$ with the ion selective electrode. A $AgNO_3$ test was used to confirm negligible chloride content in both the water washings and neat ILs. The water content of the ionic liquid was measured using a Metrohm 899 Karl-Fisher Coulometer on 0.1 mL of sample.

Inductively coupled plasma-mass spectroscopy (ICP-MS)

Quantification of lithium, potassium and silver was carried out using an inductively coupled plasma-mass spectrometer

(ICP-MS; NexION 350×, PerkinElmer, USA). Internal standards Sc (200 ppb) and Rh (20 ppb) in 1% aqua regia were used for correction of matrix effects. The internal standard solution was mixed prior to the nebulizer using a T-piece in a 1:1 ratio. Calibration standards for lithium and potassium (PerkinElmer, silver, lithium or potassium standard 1000 ppm in 2% HNO_3) were prepared at 0.1, 1, 10, 50, 100 and 500 ppb with 2% suprapur HNO_3 in each. The mass spectrometer was operated in kinetic energy discrimination mode (KED) with 50 ms dwell times, 20 sweeps, one reading and three replicates. The plasma source conditions were: nebulizer gas flow 1.02 L min^{-1}, auxiliary gas flow 1.2 L min^{-1}, plasmagas flow 15 L min^{-1}, and ICP RF power 1500 W. Data analysis was carried out using Syngistix (PerkinElmer) software. Signal responses were normalised to the scandium internal standard.

Differential scanning calorimetry (DSC)

To prepare a sample for DSC, 5–10 mg of sample was weighed into an aluminium DSC pan in an argon (Ar)-filled glove box. DSC was measured on a Netzch 214 Polyma DSC with a scan rate of 10 °C min^{-1} for three heating and cooling cycles.

Thermal gravimetric analysis (TGA)

TGA was performed on a TA-Q50 TA instruments system over a temperature range of 25 °C to 550 °C. 5–10 mg of sample was quickly loaded into a clean platinum pan in air before being inserted in the N_2 gas stream, and measurements were performed under N_2 (flow rate 40 mL min^{-1}), at a heating rate of 10 °C min^{-1}. The thermal decomposition temperature was defined as the temperature at which each material displayed 5% weight loss above 100 °C.

Density and viscosity

The density of the ionic liquids was measured using a density meter from Anton Paar (DMA 4500M) in the temperature range between 25 °C and 30 °C to 90 °C at 10 °C intervals. The ionic liquid was drawn into a syringe (1 mL) in an Ar-filled glove box and directly injected into the densitometer without being exposed to air. The error was estimated to be ±0.001 g cm^{-3}. The viscosity of the ionic liquids were measured by a rolling-ball viscometer from Anton Paar (Lovis 2000 M/ME) in the temperature range between 25 °C and 30 °C to 90 °C at 10 °C intervals with a 10 mm long capillary tube (∅1.8 mm diameter) with automatic tilted angle.

Electrochemical impedance spectroscopy (EIS)

The ionic conductivity was measured by electrochemical impedance spectroscopy (EIS) on a Biologic MTZ-35 impedance analyzer (Bio-Logic Science Instruments, France), equipped with a Eurotherm 2204e temperature controller. Samples were prepared in an Ar-filled glovebox in a custom-made conductivity dip-cell composed of two Pt electrodes, and conductivity measured in the temperature range 30 °C to 90 °C. A reference standard of 10 mM KCl solution at 30 °C was used for dip-cell measurements to determine the cell constant. All samples were equilibrated for 10 minutes per temperature and three heating and cooling cycles were performed per sample. The data was analysed by fitting with a semicircle on the Nyquist plot using MT-Lab software.

Pulsed-field gradient nuclear magnetic resonance spectroscopy

The diffusivities of the $[C_{1O1}mpip]^+$, $[C_{1O1}mmor]^+$ and Li^+ cations, $[FSI]^-$ and $[TFSI]^-$ anions for both the neat and 10 mol% Li–salt samples were determined by ^1H, ^{19}F and ^7Li pulsed-field gradient double stimulated echo (PFG-STE) NMR. The samples were packed into 5 mm NMR tubes inside an Ar-filled glovebox. The measurements were performed on a 7.05 T Bruker Avance III spectrometer equipped with a Diff50 probe. The data were recorded at 25 °C and every 10 °C from 30 to 90 °C (with a minimum of 10 min equilibration time before each measurement). The pulsed field gradient stimulated echo pulse sequence was utilised with eight scans at each gradient strength. The diffusion time (Δ) was 25 ms, gradient duration (δ) was 1 ms and the maximum gradient strength used was 2800 G cm^{-1}. The signal attenuation profiles were fitted to the Stejskal–Tanner equation[25,26] on Topspin to obtain the diffusion coefficients.

Cyclic voltammetry

Cyclic voltammetry (CV) experiments were performed using a three-electrode cell at 25 °C: a 3 mm glassy carbon (GC) working electrode, a coiled platinum wire counter electrode, and a AgOTf reference electrode. The AgOTf reference electrode was prepared from a 0.05 M solution of AgOTf and the IL being measured. The GC electrode was cleaned with 0.3 m alumina and water before each scan in the positive or negative direction. The Pt wire was cleaned by flame. CV analysis was carried out on a Biologic SP-200 potentiostat inside a glovebox with an Ar atmosphere. The reductive scans were conducted before the oxidative scans. Ferrocene was used to normalise the reference potential *vs.* Ag/Ag^+.

Fourier transform infrared spectroscopy

The vibrational spectral features of the materials were obtained from FTIR spectroscopy using a single diamond Attenuated Total Refection (ATR) unit (PerkinElmer) running on Spectrum software. The spectra were collected from 1500 cm^{-1} to 450 cm^{-1} under an Ar atmosphere (only the relevant regions of the spectra have been presented herein). Approximately 10 mg of each sample was placed on the sensing surface of the spectrometer and pressure applied to ensure that there was sufficient contact before each spectrum was acquired at a spectral resolution of 4 cm^{-1} with 32 co-added scans. Spectral data was deconvoluted on Origin 2019 with Gaussian profiles.

Raman spectroscopy

The interactions between Li^+ and TFSI anions of ionic liquid electrolytes were analysed with Raman spectroscopy. Calibration electrolytes were prepared of 5, 7.5, 10, 15 and 20 mol% LiTFSI in $[C_{1O1}mpip][TFSI]$ and $[C_{1O1}mmor][TFSI]$ and dried at 60 °C under vacuum for 48 h. Samples were sealed under Ar between a microscope slide and a quartz cover slip using melted parafilm to avoid exposure to water. The samples were

stored under Ar until analysed. Raman spectra of the prepared solutions were collected using a Renishaw inVia Raman Microscope equipped with a near-IR 785 nm diode laser through a 20-power objective lens (Leica, 0.40 NA, 1.1 mm), leading to a 2.29 μm spot size at room temperature. For each calibration solution, the spectra were recorded with a 740 cm^{-1} center at 1% laser power, 10 second exposure and 250 acquired spectra. Using Renishaw WiRE 3.4 software, the background was removed and normalised. Spectral data was deconvoluted on CasaXPS with 40 : 60 Gaussian : Lorentzian fixed profiles.

Fitting of the transport properties

Transport properties of the neat ionic liquids and the Li–salt mixtures were fitted with the Vogel–Tammann–Fulcher (VTF) equation (eqn (1)), which is often used to describe the temperature-dependence of IL transport properties in a broad temperature range.[27]

$$\Upsilon = \Upsilon_0 \exp\left(\frac{B^{\Upsilon}}{T - T_0^{\Upsilon}}\right) \quad (1)$$

where Υ is the transport property related to dynamics, *e.g.* dynamic viscosity (η), specific conductivity (κ), molar conductivity (Λ_{imp} or Λ_{NMR}). Υ, B_Υ, and $T_{0,\Upsilon}$ (the Vogel temperature) are material dependent fitting parameters. The VTF equation describes empirical relationships but extrapolation down to a materials' T_g value increases the uncertainty as experiments were only measured from 25 °C. The Angell's strength parameter (δ_Υ), a measure of the liquid fragility of glass formers, is the pseudoactivation energy, B_Υ, scaled against the ideal glass transition temperature, $T_{0,\Upsilon}$ ($\delta_\Upsilon = B_\Upsilon/T_{0,\Upsilon}$) and describes the rate of change in a transport property upon change in temperature.[27–29] In narrow temperature ranges (25–60 °C) a linear fit was possible with R^2 values above 0.99 for transport properties reported, where the Arrhenius equation (eqn (2)) can be used to determine the activation energy of a transport process.[30]

$$\ln(\Upsilon) = \ln(\Upsilon_0) - \frac{E_{a,\Upsilon}}{RT} \quad (2)$$

where $E_{a,\Upsilon}$ is the activation energy for ion transport by migration, of the transport property Υ and is calculated from the slope of the Arrhenius plot.

Synthesis

***N*-Methoxymethyl-*N*-methylpiperidinium chloride, [C_{1O1}mpip]Cl.** Chloromethylmethyl ether (2.00 g, 25 mmol) was added dropwise over 30 minutes to a stirring solution of *N*-methylpiperidine (2.71 g, 27 mmol) and acetone (20 mL) under an inert atmosphere at 0 °C. The reaction was stirred for 24 h at room temperature. The solution was filtered, and the solid material was washed with acetone (3 × 20 mL). The solid was then dried *in vacuo* at 50 °C to yield *N*-methoxymethyl-*N*-methylpiperidinium chloride as a white solid (3.20 g, 57% yield). ^{1}H NMR (DMSO-d_6, 200 MHz): δ 4.69 (s, 2H, NCH_2O), 3.62 (s, 3H, OCH_3), 3.28 (m, 4H, CH_2CH_2N), 2.98 (s, 3H, NCH_3), 1.78 (m, 4H, CH_2CH_2N), 1.65–1.45 (m, 2H, C$H_2CH_2CH_2$N) ppm. ^{13}C NMR (DMSO-d_6, 100 MHz): δ 92.05 (NCH_2O), 61.42 (OCH_3), 55.86 (CH_2CH_2N), 44.58 (NCH_3), 21.34 ($CH_2CH_2CH_2$N), 19.33 (CH_2CH_2N) ppm. ES$^+$ *m*/*z* 144.0 $(C_8H_{18}NO)^+$, ES$^-$ *m*/*z* 34.8 (Cl^-). Anal. calculated for $C_8H_{18}NOCl$; C, 53.47; H, 10.10; N, 7.80; found: C, 53.15; H, 10.04; N, 7.86.

***N*-Methoxymethyl-*N*-methylpiperidinium bis(fluorosulfonyl) imide, [C_{1O1}mpip][FSI].** [C_{1O1}mpip]Cl (10.00 g, 56 mmol) and KFSI (12.44 g, 57 mmol) were dissolved separately in Milli-Q water (2 × 75 mL) and the solutions were stirred together for 3 h. DCM (50 mL) was added to the flask and the two layers were separated. The organic layer was washed with Milli-Q water (6 × 20 mL) and the organic solvent was evaporated. The resulting liquid was then dried *in vacuo* at 60 °C to yield *N*-methoxymethyl-*N*-methylpiperidinium bis(fluorosulfonyl)imide as a colourless liquid (15.64 g, 87% yield). ^{1}H NMR (DMSO-d_6, 200 MHz): δ 4.65 (s, 2H, NCH_2O), 3.61 (s, 3H, OCH_3), 3.25 (m, 4H, CH_2CH_2N), 2.95 (s, 3H, NCH_3), 1.78 (m, 4H, CH_2CH_2N), 1.64–1.44 (m, 2H, C$H_2CH_2CH_2$N) ppm. ^{13}C NMR (DMSO-d_6, 100 MHz): δ 92.11 (NCH_2O), 61.41 (OCH_3), 55.93 (CH_2CH_2N), 44.61 (NCH_3), 21.33 ($CH_2CH_2CH_2$N), 19.31 (CH_2CH_2N) ppm. ^{19}F NMR (DMSO-d_6, 376.5 MHz): δ 53.21 ppm. ES$^+$ *m*/*z* 144.0 $(C_8H_{18}NO)^+$, ES$^-$ *m*/*z* 179.9 (FSI^-). Anal. calculated for $C_8H_{18}N_2O_5S_2F_2$; C, 29.62; H, 5.59; N, 8.64; found: C, 29.64; H, 3.45; N, 8.30. No white precipitates with $AgNO_3$ test. Potassium content (ICP) 10 ppm.

***N*-Methoxymethyl-*N*-methylpiperidinium bis(trifluoromethanesulfonyl)imide, [C_{1O1}mpip][TFSI].** [C_{1O1}mpip]Cl (10.07 g, 56 mmol) and LiFSI (16.41 g, 57 mmol) were dissolved separately in Milli-Q water (2 × 75 mL) and the solutions were stirred together for 3 h. DCM (50 mL) was added to the flask and the two layers were separated. The organic layer was washed with Milli-Q water (6 × 20 mL) and the organic solvent was evaporated. The resulting liquid was then dried *in vacuo* at 60 °C to yield *N*-methoxymethyl-*N*-methylpiperidinium bis(trifluoromethanesulfonyl)imide as a colourless liquid (21.94 g, 92% yield). ^{1}H NMR (DMSO-d_6, 200 MHz): δ 4.65 (s, 2H, NCH_2O), 3.61 (s, 3H, OCH_3), 3.25 (m, 4H, CH_2CH_2N), 2.95 (s, 3H, NCH_3), 1.78 (m, 4H, CH_2CH_2N), 1.66–1.41 (m, 2H, C$H_2CH_2CH_2$N) ppm. ^{13}C NMR (DMSO-d_6, 100 MHz): δ 119.47 (CF_3, J_{CF} = 320.07 Hz), 91.63 (NCH_2O), 60.93 (OCH_3), 56.43 (CH_2CH_2N), 44.12 (NCH_3), 20.85 ($CH_2CH_2CH_2$N), 18.83 (CH_2CH_2N) ppm. ^{19}F NMR (DMSO-d_6, 376.5 MHz): δ −78.71 (CF_3) ppm. ES$^+$ *m*/*z* 144.2 $(C_8H_{18}NO)^+$, ES$^-$ *m*/*z* 280.0 ($TFSI^-$). Anal. calculated for $C_{10}H_{18}N_2O_5S_2F_6$; C, 28.30; H, 4.28; N, 6.60; found: C, 28.49; H, 4.40; N, 6.98. No white precipitates with $AgNO_3$ test. Lithium content (ICP) below limit of detection.

***N*-Methoxymethyl-*N*-methylmorpholinium chloride, [C_{1O1}mmor]Cl.** Chloromethylmethyl ether (2.50 g, 31 mmol) was added dropwise over 30 minutes to a stirring solution of *N*-methylmorpholine (3.46 g, 34 mmol) and acetonitrile (20 mL) under an inert atmosphere in a round-bottom flask fitted with a reflux condenser at 50 °C. The reaction was stirred for 3 h at 50 °C. The solution was filtered, and the solid material was washed with acetonitrile (3 × 20 mL). The solid was then dried *in vacuo* at 50 °C to yield *N*-methoxymethyl-*N*-methylmorpholinium chloride as a white solid (3.20 g, 57% yield). ^{1}H NMR (DMSO-d_6, 200 MHz): δ 4.84 (s, 2H, NCH_2O), 3.93 (m, 4H, CH_2OCH_2), 3.64 (s, 3H, OCH_3), 3.44 (t, 4H, CH_2CH_2N), 3.15 (s, 3H, NCH_3) ppm. ^{13}C NMR (DMSO-d_6, 100 MHz): δ 92.18 (NCH_2O), 61.11 (OCH_3), 59.46 (CH_2OCH_2), 55.06 (CH_2CH_2N), 43.28 (NCH_3) ppm. ES$^+$ *m*/*z* 145.9

$(C_7H_{16}NO_2)^+$, ES$^-$ *m*/*z* 34.8 (Cl^-). Anal. calculated for $C_7H_{16}NO_2Cl$; C, 46.28; H, 8.88; N, 7.71; found: C, 46.29; H, 8.86; N, 7.70.

***N*-Methoxymethyl-*N*-methylmorpholinium bis(fluorosulfonyl) imide, [C$_{1O1}$mmor][FSI].** [C_{1O1}mmo]Cl (2.50 g, 14 mmol) and KFSI (3.32 g, 15 mmol) were dissolved separately in Milli-Q water (2 × 10 mL) and the solutions were stirred together for 24 h. DCM (20 mL) was added to the flask and the two layers were separated. The organic layer was washed with Milli-Q water (7 × 10 mL) and the organic solvent was evaporated. The resulting liquid was then dried *in vacuo* at 60 °C to yield *N*-methoxymethyl-*N*-methylmorpholinium bis(fluorosulfonyl)imide as a colourless liquid (3.31 g, 74% yield). ^{1}H NMR (DMSO-d$_6$, 200 MHz): δ 4.75 (s, 2H, NCH_2O), 3.93 (m, 4H, CH_2OCH_2), 3.63 (s, 3H, OCH_3), 3.47–3.26 (m, 4H, CH_2CH_2N), 3.11 (s, 3H, NCH_3) ppm. ^{13}C NMR (DMSO-d$_6$, 200 MHz): δ 92.59 (NCH_2O), 61.15 (OCH_3), 59.50 (CH_2OCH_2), 55.24 (CH_2CH_2N), 43.48 (NCH_3) ppm. ^{19}F NMR (DMSO-d$_6$, 376.5 MHz): δ 53.23 ppm. ES$^+$ *m*/*z* 146.1 $(C_7H_{16}NO_2)^+$, ES$^-$ *m*/*z* 179.9 (FSI^-). Anal. calculated for $C_7H_{16}N_2O_6S_2F_2$; C, 25.76; H, 4.94; N, 8.58; found: C, 26.06; H, 4.69; N, 8.29. No white precipitates with $AgNO_3$ test. Potassium content (ICP) 15 ppm.

***N*-Methoxymethyl-*N*-methylmorpholinium bis(trifluoromethanesulfonyl)imide, [C$_{1O1}$mmor][TFSI].** [C_{1O1}mmo]Cl (1.80 g, 10 mmol) and LiTFSI (3.12 g, 11 mmol) were dissolved separately in Milli-Q water (2 × 10 mL) and the solutions were stirred together for 24 h. DCM (20 mL) was added to the flask and the two layers were separated. The organic layer was washed with Milli-Q water (3 × 10 mL) and the organic solvent was evaporated. The resulting liquid was then dried *in vacuo* at 60 °C to yield *N*-methoxymethyl-*N*-methylmorpholinium bis(trifluoromethanesulfonyl)imide as a colourless liquid (3.34 g, 79% yield). ^{1}H NMR (DMSO-d$_6$, 200 MHz): δ 4.76 (s, 2H, NCH_2O), 3.93 (m, 4H, CH_2OCH_2), 3.63 (s, 3H, OCH_3), 3.41–3.32 (m, 4H, CH_2CH_2N), 3.11 (s, 3H, NCH_3) ppm. ^{13}C NMR (DMSO-d$_6$, 200 MHz): δ 119.48 (CF_3, J_{CF} = 319.89 Hz), 92.57 (NCH_2O), 61.16 (OCH_3), 59.49 (CH_2OCH_2), 55.21 (CH_2CH_2N), 43.45 (NCH_3) ppm. ^{19}F NMR (DMSO-d$_6$, 376.5 MHz): δ −78.74 (CF_3) ppm. ES$^+$ *m*/*z* 146.1 $(C_7H_{16}NO_2)^+$, ES$^-$ *m*/*z* 279.9 ($TFSI^-$). Anal. calculated for $C_9H_{16}N_2O_6S_2F_6$; C, 25.35; H, 3.78; N, 6.57; found: C, 25.41; H, 3.58; N, 6.40. No white precipitates with $AgNO_3$ test. Lithium content (ICP) 32 ppm.

Results and discussion

Thermal properties

The thermal properties of ILs are important as they determine the temperature range in which they can operate as liquid electrolytes. The lower temperature limit that an electrochemical device can operate at is defined by the melting point (T_m) or glass transition temperature (T_g) of the IL, below which the crystallinity or amorphous phase of the material restricts the ion mobility and therefore, ion conduction. The differential scanning calorimetry (DSC) traces for both pure IL and ILs containing 10 mol% Li salt are reported in Fig. 2 and Table 1 summarises the thermal properties in terms of glass transition (T_g), cold crystallisation (T_{cc}), melting (T_m) and decomposition (T_d) temperatures.

There are three types of thermal behaviour commonly observed in ILs based on their kinetics under the specific measurement conditions (*e.g.* scan rate).[31] The first kind of thermal behaviour presents only glass transitions, resulting in liquids above the T_g and glasses below the T_g. Two of the new ILs are in this first type, [C_{1O1}mmor][TFSI] and [C_{1O1}mpip][TFSI]. The second type undergoes crystallisation on cooling and melts on heating, and [C_{1O1}mpip][FSI] is categorised in this class. The third type undergoes a cold crystallisation and melting on heating, which is observed for [C_{1O1}mmor][FSI].

All the samples show glass-transition temperatures (T_g) in the temperature range measured, except for [C_{1O1}mpip][FSI], although upon addition of LiFSI to [C_{1O1}mpip][FSI] a T_g appears. The T_g of the TFSI-based ILs is increased upon addition of LiTFSI. Only the FSI-based ILs show a T_m, which is suppressed upon the addition of LiFSI, which widens the temperature range of the material and thus allows for expanded application ranges.

There is a complete absence of ordered crystalline structure in the TFSI-based ILs, which leads only to the formation of amorphous glasses at the T_g. The absence of a melting

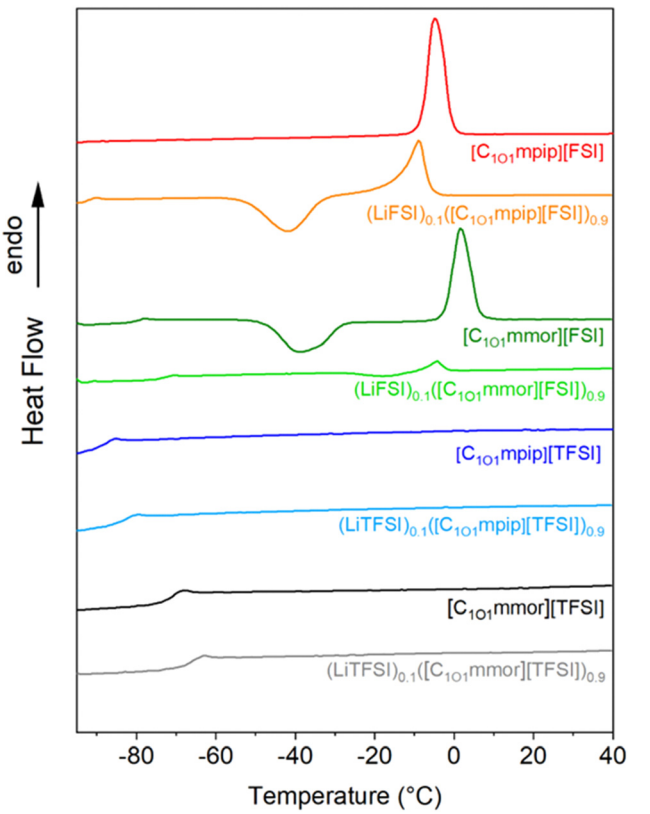

Fig. 2 DSC thermograms showing the second heating cycle for [TFSI]-based ionic liquids and their 10 mol% LiTFSI solutions and [FSI]-based ionic liquids and their 10 mol% LiFSI solutions.

Table 1 Thermal behaviour of ILs, data extracted from DSC and TGA. T_m and T_{cc} values were extracted from peak onsets on DSC curve and T_g values were extracted from the midpoint of the T_g

Ionic liquid	$T_g \pm 1$ (°C)	$T_{cc} \pm 1$ (°C)	$T_m \pm 1$ (°C)	$T_{d(5\% \text{ weight loss})} \pm 1$ (°C)
$[C_{1O1}mpip][FSI]$	—	−59	−8	238
$(LiFSI)_{0.1}([C_{1O1}mpip][FSI])_{0.9}$	−94	−53	−26	
$[C_{1O1}mmor][FSI]$	−79	−50	−2	219
$(LiFSI)_{0.1}([C_{1O1}mmor][FSI])_{0.9}$	−75	−27	−10	
$[C_{1O1}mpip][TFSI]$	−80	—	—	282
$(LiTFSI)_{0.1}([C_{1O1}mpip][TFSI])_{0.9}$	−79	—	—	
$[C_{1O1}mmor][TFSI]$	−69	—	—	248
$(LiTFSI)_{0.1}([C_{1O1}mmor][TFSI])_{0.9}$	−64	—	—	

transition has also been observed in $[C_{2O2}mmor][TFSI]$ and $[C_{2O2}mpip][TFSI]$, which the authors attributed to the flexibility of the ether side chain.[32] Given that the FSI anions coupled with the smaller ether chain cations allowed crystallisation of the IL whereas the TFSI-based ILs are liquids it would appear that the size of the TFSI anion suppresses crystallisation in the TFSI-based ILs. This idea is further supported by the presence of a melting transition in the thermal analysis of the alkyl equivalent *N*-propyl-*N*-methylpiperidinium IL, $[C_3mpip][TFSI]$ (T_m = 12.3 °C)[33] but not in *N*-propyl-*N*-methylmorpholinium IL, $[C_3mmor][TFSI]$.[34]

$[C_{1O1}mpip][TFSI]$ has the lowest T_g at −80 °C and there was no T_g observed for $[C_{1O1}mpip][FSI]$ in the temperature range studied (lower limit of −100 °C). The shorter alkoxy chain has resulted in lower T_g for both $[C_{1O1}mpip][TFSI]$ and $[C_{1O1}mmor][TFSI]$ (−80 and −69 °C, respectively) compared longer alkoxy chain cations such as *N*-ethoxyethyl-*N*-methylpiperidinium IL, $[C_{2O2}mpip][TFSI]$ and *N*-ethoxyethyl-*N*-methylmorpholinium $[C_{2O2}mmor][TFSI]$, with T_g values of −78 and −62 °C, respectively.[32]

The presence of an oxygen has decreased the melting temperature of $[C_{1O1}mpip][FSI]$ (T_m −8 °C) compared to the alkyl-equivalent $[C_3mpip][FSI]$, which has a T_m of 4 °C and T_g of −94 °C, attributed to the enhanced conformational degrees of freedom of the alkoxy chain.[35] Supercooling is a common finding in ILs, especially in ether-functionalised ILs,[36] and a cold crystallisation is observed in the DSC heating traces of $[C_{1O1}mmor][FSI]$ and $(LiFSI)_{0.1}([C_{1O1}mpip][FSI])_{0.9}$. Addition of a higher molar concentration of LiFSI would most likely supress the melt entirely, thus widening the liquid range of these FSI-based electrolytes further.

Thermogravimetric analysis (TGA) measurements were performed as an initial assessment of thermal stability and are reported in Table 1 and the mass loss traces are shown in Fig. S1 (ESI†). Decomposition temperatures (T_d) were determined at a mass loss of 5%. All the neat ILs show decomposition above 200 °C. Both FSI-based ILs show a one-stage decomposition whilst TFSI-based ILs show a two-stage decomposition and are more thermally stable. The TFSI anion and piperidinium cation are most thermally stable, ergo $[C_{1O1}mpip][TFSI]$ has highest T_d whilst $[C_{1O1}mmor][FSI]$ has lowest T_d. A decrease in T_d is observed compared to piperidinium cations with no oxygens and cations with longer ethoxy chains, *e.g.* *N*-butyl-*N*-methylmorpholinium TFSI $[C_4mmor][TFSI]$ and *N*-methoxyethyl-*N*-methylmorpholinium TFSI $[C_{1O2}mmor][TFSI]$, have T_d values of 398 and 387 °C, respectively.[37,38] Whereas the decomposition temperature of $[C_{1O1}mmor][TFSI]$ (T_d = 219 °C) is similar to its alkyl analogue $[C_3mmor][TFSI]$, which has a T_d of 200 °C.[34]

The length of the alkoxy chain has a significant impact on the decomposition temperatures of these materials, with shorter chains having the lowest decomposition temperatures in each cation family.[9,10] Even so, the TGA results show that all four ILs are stable above 200 °C which is adequate thermal stability for most electrochemical applications.

Density

Density measurements of the ILs and electrolyte solutions were performed between 25–90 °C and the experimental data summarised in Fig. 3 and Tables S1, S2 (ESI†). The densities are lower with the $[FSI]^-$ anion and $[C_{1O1}mpip]^+$ cation. The density difference upon changing the cation from piperidinium to morpholinium has a larger effect than changing the anion, despite the minimal change in molecular weight. Since the cation molecular weights are very similar, the higher densities of the morpholinium ILs must be rationalised with structural changes on the molecular level directly resulting from the oxygen on the cation ring. The oxygen on the ring is more electron rich than the oxygen on the chain,[39] and likely interacts with other organic cations and anions resulting in a decrease in interionic separation and increase in efficient packing.

The methoxymethyl chain results in higher densities than for longer ether-functionalised cations, due to more efficient packing with shorter chains, and the equivalent alkyl-functionalised ILs, for example at 25 °C $[C_{1O1}mpip][FSI]$ and $[C_{1O1}mpip][TFSI]$ have densities of 1.39 and 1.47 g cm^{-3},

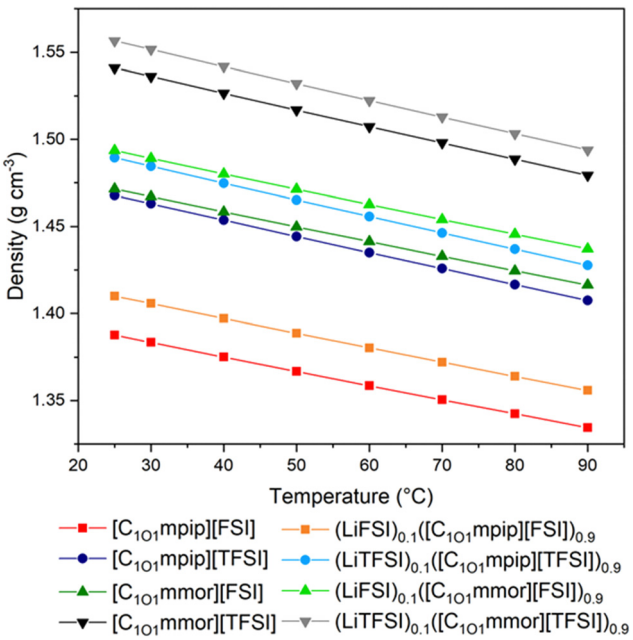

Fig. 3 Temperature dependence of the density for the neat ILs and their electrolytes.

respectively, compared to 1.32 and 1.41 g cm^{-3} for [C_3mpip][FSI] and [C_3mpip][TFSI], respectively.[33,40] In all cases, the addition of Li–salt resulted in a similar increase in density of around 0.02 g cm^{-3} at any given temperature.

Transport properties

Viscosity. Viscosity (η) is an important parameter for ILs as it is correlated to rate of mass transport and is influenced by various factors such as cation and anion species.[41] The viscosity can significantly impact the diffusion coefficient of species in the electrolyte solution and therefore limit charge/discharge rates and electrochemical reactions. The viscosities of the neat ILs and their electrolyte solutions were measured between 25–90 °C and the experimental data is presented in Fig. 4 and Table S3 (ESI†). The Arrhenius plot for the viscosity data shows a curvature, suggesting a temperature dependence of the activation energy (Fig. 4) and therefore the data was fit to the VTF equation (eqn (1)). The VTF plot for viscosities is shown in Fig. S2 (ESI†). The VTF fitting parameters are reported in Table 2, along with viscosities of the ILs at 30 °C, the Angell strength parameter δ_η and activation energy $E_{a,\eta}$ obtained from the Arrhenius equation (eqn (2)) in the range 25–60 °C. The Angell strength parameter values, δ_η, a measure for liquid fragility, are in a narrow range from 3.3 to 5.7 and do not reveal a general trend but are consistent with fragile glass-forming liquids.[27,42,43] Fragility describes the rate at which transport properties change with temperature close to the T_g. Strong glass formers such as SiO_2 and GeO_2 more closely follow the Arrhenius equation (eqn (2)), while fragile glass formers exhibit large deviations from it.[27,44] The activation energies, $E_{a,\eta}$, which represent the energy required for viscous flow and are related to the macroscopic frictional force in the system, show the same trend as the viscosities across the different ILs/electrolytes studied.

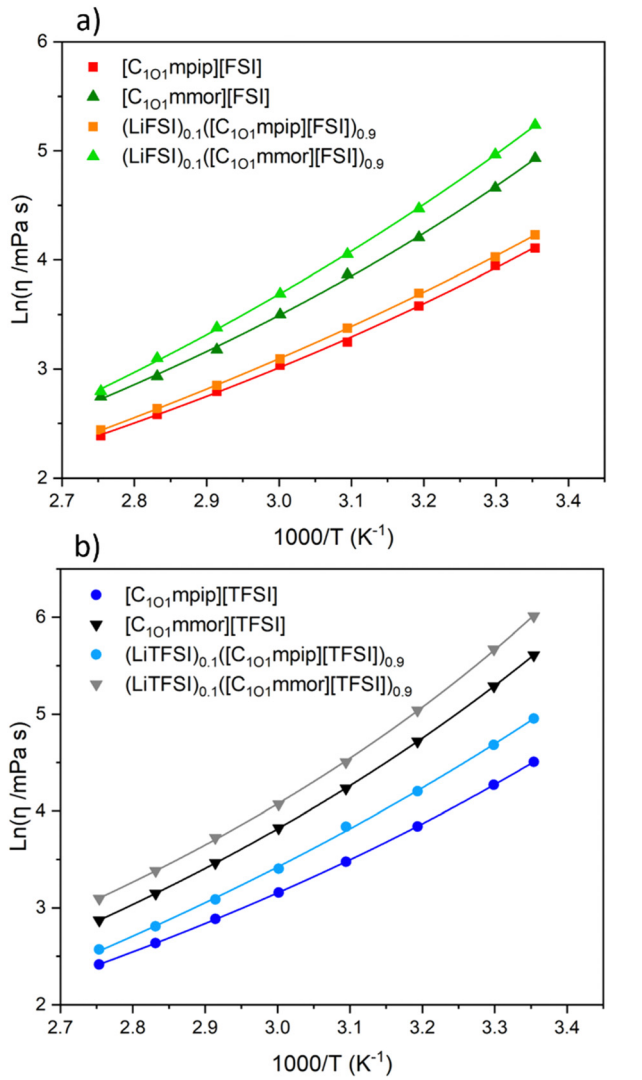

Fig. 4 Temperature dependent viscosity plots of (a) FSI-based ionic liquids and their 10 mol% LiFSI electrolyte solutions and (b) TFSI-based ionic liquids and their 10 mol% LiTFSI electrolyte solutions.

At 30 °C, the piperidinium-based ILs have significantly lower viscosities than the morpholinium ILs. For all samples, the addition of Li–salt increases the viscosity, but has a smaller impact on FSI-based ILs than TFSI-based ILs. The viscosities depend on the molecular weight of the anion, and the structures of the cations. It is well known that the FSI anion leads to lower viscosity ILs than TFSI and the same is true for the ILs with both cations here.[45] The largest factor affecting viscosity is found to be the cation structure. By changing the piperidinium cation to morpholinium cation, the viscosity increased by a factor of 2.04 for the FSI-based ILs and 2.77 for the TFSI-based ILs at 30 °C. In comparison, a change of anion from FSI to TFSI in the piperidinium and morpholinium-based ILs led to an increase in factor of 1.38 and 1.87, respectively. Unlike the oxygen on the chain, which lowers viscosity (for example, at 25 °C the viscosities of [C_{1O1}mpip][FSI] and [C_{1O1}mpip][TFSI] are 61 and 91 mPa s respectively, compared to [C_3mpip][FSI] and [C_3mpip][TFSI] which are 95 and 147 mPa s respectively),[46] the second oxygen on the ring more than doubles the viscosity.

The methoxymethyl chain has increased viscosity compared to the ethoxymethyl chain: [C_{2O1}mmor][TFSI] and [C_{2O1}mpip][TFSI] have viscosities of 258 mPa s and 70 mPa s, at 25 °C respectively.[47] The reason for slightly increased viscosity with the methoxymethyl chain is believed to be the cation conformations, whereby the longer ether chain (ethoxymethyl) has a higher degree of conformational freedom and can curl around the centre of the cation, leading to a more spherical cation, simultaneously shielding the positively charged nitrogen centre more effectively than the shorter methoxymethyl chain.[48–50] The shielding thus leads to reduced interactions between the cation and anion. Furthermore, long ether-functionalised chains have high conformational flexibility which creates more free volume compared to alkyl chains.[51]

Addition of Li–salt increased viscosity, as expected. The interactions between $TFSI^-$ and Li^+ are stronger than between FSI^- and Li^+, which results in a larger increase in viscosity for the TFSI-based ILs.[45,52,53] For both cation systems, the FSI-based electrolytes have smaller increase in viscosity upon Li salt addition compared to the TFSI-based electrolytes. At 30 °C there is an increase in viscosity of less than 40 mPa s for all electrolytes, except for $(LiTFSI)_{0.1}([C_{1O1}mmor][TFSI])_{0.9}$ which

Table 2 Viscosity of the pure ionic liquids, VTF fitting parameters (η_0, B_η, $T_{0,\eta}$), Angell strength factor δ_η and activation energy $E_{a,\eta}$ (in the range 25 to 60 °C) for the T-dependent viscosity

Ionic liquid	$\eta^{30\,°C}$/mPa s	$\eta_0/10^{-1}$ mPa s	B_η/K	$T_{0,\eta}$/K	δ_η	$E_{a,\eta}$/kJ mol^{-1}
$[C_{1O1}mpip][FSI]$	52	4.1 ± 0.6	625 ± 141	174 ± 17	3.6	26
$(LiFSI)_{0.1}([C_{1O1}mpip][FSI])_{0.9}$	56	2.3 ± 0.8	802 ± 70	157 ± 7	5.1	27
$[C_{1O1}mmor][FSI]$	106	3.6 ± 0.6	659 ± 123	188 ± 12	3.5	33
$(LiFSI)_{0.1}([C_{1O1}mmor][FSI])_{0.9}$	144	1.5 ± 0.7	897 ± 109	172 ± 9	5.2	37
$[C_{1O1}mpip][TFSI]$	72	2.5 ± 1.0	696 ± 13	180 ± 1	3.9	32
$(LiTFSI)_{0.1}([C_{1O1}mpip][TFSI])_{0.9}$	108	1.0 ± 0.5	947 ±190	167 ± 16	5.7	36
$[C_{1O1}mmor][TFSI]$	198	2.1 ± 1.0	760 ± 11	192 ± 1	4.0	42
$(LiTFSI)_{0.1}([C_{1O1}mmor][TFSI])_{0.9}$	290	3.4 ± 0.8	664 ± 46	205 ± 4	3.3	46

has a >90 mPa s increase in viscosity compared to the neat IL. The pseudoactivation energy B_η has increased upon addition of Li–salt for all electrolytes except for $(LiTFSI)_{0.1}([C_{1O1}mmor][TFSI])_{0.9}$ (where a decrease in B_η but an increase in $T_{0,\eta}$ is observed), resulting in higher δ_η. This suggests the addition of Li–salt results in ions requiring a larger amount of energy to diffuse past each other, which is related to their inherently high viscosities.

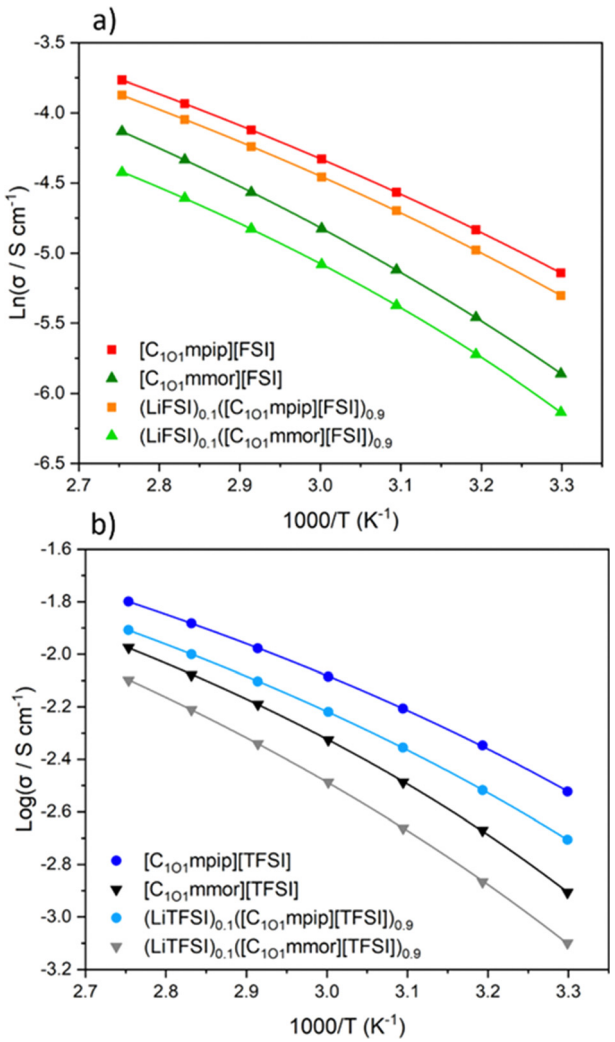

Fig. 5 Temperature dependent ionic conductivity plots of (a) FSI-based ionic liquids and their 10 mol% LiFSI electrolyte solutions and (b) TFSI-based ionic liquids and their 10 mol% LiTFSI electrolyte solutions.

Conductivity. Determining the ionic conductivity of new electrolytes is important as it is a key parameter influencing the overall performance of a battery electrolyte. The ionic conductivity (σ) of the pure ILs and Li–salt solutions were measured from 30 °C to 90 °C and the results are reported in Fig. 5 and Table S4 (ESI†), organised by anion type. The VTF plot for conductivities is shown in Fig. S3 (ESI†). The VTF fitting parameters for conductivity and molar conductivity are summarised in Table S5 (ESI†) and Table 3, respectively. The VTF parameter σ_0 represents the ionic conductivity at infinite temperature and the pseudoactivation energy, B_σ, is related to the critical free volume for ion transport. The molar conductivities are presented in Table S6 (ESI†). The $\delta_{\Lambda imp}$ values again show no trend and are between 2.4 and 4.4; the small range is expected considering the similar cationic and anionic structures.[43]

All the neat ILs exhibited conductivities above 10^{-3} S cm^{-1} in the temperature range measured. However, $(LiTFSI)_{0.1}([C_{1O1}mmor][TFSI])_{0.9}$ was lower at 8×10^{-4} S cm^{-1}, which originates from the low ionic conductivity of the pure IL, $[C_{1O1}mmor][TFSI]$. The highest conductivity at 30 °C was found for $[C_{1O1}mpip][FSI]$ at 5.9×10^{-3} S cm^{-1}, which was almost retained upon addition of LiFSI, at 5.0×10^{-3} S cm^{-1}. The higher conductivities for the FSI-based ILs are attributed to the smaller size of the anion and the higher tendency of $[FSI]^-$ anions to dissociate compared to $[TFSI]^-$ anions.[54] The conductivity of the neat FSI IL was reduced upon changing the cation to $[C_{1O1}mmor]^+$, to 2.8×10^{-3} S cm^{-1}, and similarly reduced when changing the anion to TFSI.

The ether-functionality has enhanced the ionic conductivity of the piperidinium-based ILs compared to their alkyl counterparts: $[C_3mpip][FSI]$ and $[C_3mpip][TFSI]$, have conductivities of 3.7×10^{-3} and 1.4×10^{-3} S cm^{-1} at 25 °C respectively,[46] whilst $[C_{1O1}mpip][FSI]$ and $[C_{1O1}mpip][TFSI]$ have conductivities of 5.9×10^{-3} and 3.0×10^{-3} S cm^{-1} at 30 °C, respectively, attributed primarily to their lower viscosities.

The activation energy, $E_{\Lambda imp}$, calculated from eqn (2), for ILs with the $[C_{1O1}mmor]^+$ cation is higher compared to those with the $[C_{1O1}mpip]^+$ cation and further indicates that a higher thermal energy is required to achieve the same ion mobility with the $[C_{1O1}mmor]^+$ cation. Likewise, $E_{\Lambda imp}$ increases upon addition of the Li–salt for all samples.

Table 3 Calculated values for the molar conductivity at 30 °C, VTF fitting parameters, Angell strength factor and activation energy (in the range 30 to 60 °C)

Ionic liquid	$\Lambda_{imp}^{30\,^{\circ}C}$/S cm^2 mol^{-1}	$\Lambda_{imp,0}$/S cm^2 mol^{-1}	$B_{\Lambda imp}$/K	$T_{0,\Lambda imp}$/K	$\delta_{\Lambda imp}$	$E_{\Lambda imp}$/kJ mol^{-1}
$[C_{1O1}mpip][FSI]$	1.4	161 ± 1	679 ± 14	161 ± 2	4.2	23
$(LiFSI)_{0.1}([C_{1O1}mpip][FSI])_{0.9}$	1.1	130 ± 1	648 ± 24	167 ± 3	3.9	24
$[C_{1O1}mmor][FSI]$	0.6	137 ± 1	661 ± 16	180 ± 2	3.7	30
$(LiFSI)_{0.1}([C_{1O1}mmor][FSI])_{0.9}$	0.4	52 ± 1	477 ± 13	202 ± 2	2.4	33
$[C_{1O1}mpip][TFSI]$	0.9	119 ± 1	558 ± 37	190 ± 5	2.9	29
$(LiTFSI)_{0.1}([C_{1O1}mpip][TFSI])_{0.9}$	0.6	114 ± 1	584 ± 14	193 ± 2	3.0	32
$[C_{1O1}mmor][TFSI]$	0.3	90 ± 1	519 ± 27	210 ± 3	2.5	38
$(LiTFSI)_{0.1}([C_{1O1}mmor][TFSI])_{0.9}$	0.2	159± 1	723 ± 33	194 ± 3	3.7	40

Self-diffusion coefficients

The transfer of the active species, Li^+ is a prerequisite for operating lithium batteries. To understand individual ion movements at a molecular level, PFG-NMR spectroscopy was employed to measure self-diffusion coefficients of the cations (^1H or ^7Li) and anions (^{19}F). Fig. 6 shows the self-diffusion coefficients against reciprocal temperature for the neat ILs and electrolyte solutions, and Table 4 presents ion activation energies and Table S9 (ESI†) shows the self-diffusion coefficients for ^1H, ^{19}F and ^7Li for the neat ILs and electrolyte solutions at 30 °C, and the diffusivity ratios of Li^+ and example PFG NMR attenuation curves are presented in Fig. S4 (ESI†).

The $[C_{1O1}mpip]^+$ has larger $D_s(^1H)$ values than $[C_{1O1}mmor]^+$ in all cases. For the temperature dependent self-diffusion coefficients of the neat ILs, the general trend for TFSI-based ILs is that the cation diffuses faster, and for FSI-based ILs, the anion diffuses faster. The FSI^- anion leads to faster anion diffusion in both the neat ILs and their electrolytes, which is also the case for other FSI-based ILs, such as *N*-propyl-*N*-methylpyrrolidinium IL $[C_3mpyr][FSI]$,[55] as well as faster Li^+ diffusion.

Upon addition of Li–salt, the diffusion coefficients decrease for all ions, with Li^+ having the slowest diffusion coefficient except in $(LiFSI)_{0.1}([C_{1O1}mmor][FSI])_{0.9}$, where Li^+ and the IL cation have similar diffusion coefficients. The ratios of $D_s(^7Li)/D_s(^1H)$ and $D_s(^7Li)/D_s(^{19}F)$ are presented in Fig. S5 (ESI†). The highest $D_s(^7Li)$ value is observed in $(LiFSI)_{0.1}([C_{1O1}mpip][FSI])_{0.9}$ at 1.6×10^{-11} m^2 s^{-1}, which correlates to this electrolyte showing the highest conductivity. It is clear from Fig. 6 that $(LiTFSI)_{0.1}([C_{1O1}mpip][TFSI])_{0.9}$ (Fig. 6g), has a larger difference between the diffusion rate of lithium $D_s(^7Li)$ (5.1×10^{-12} m^2 s^{-1} at 30 °C) and that of the cation or anion, $D_s(^1H)$ and $D_s(^{19}F)$ (1.2×10^{-11} and 8.1×10^{-12} m^2 s^{-1} respectively, at 30 °C) than for other electrolytes (Fig. 6e, f and h). In the neat IL, $[C_{1O1}mpip][TFSI]$ has $D_s(^1H)$ and

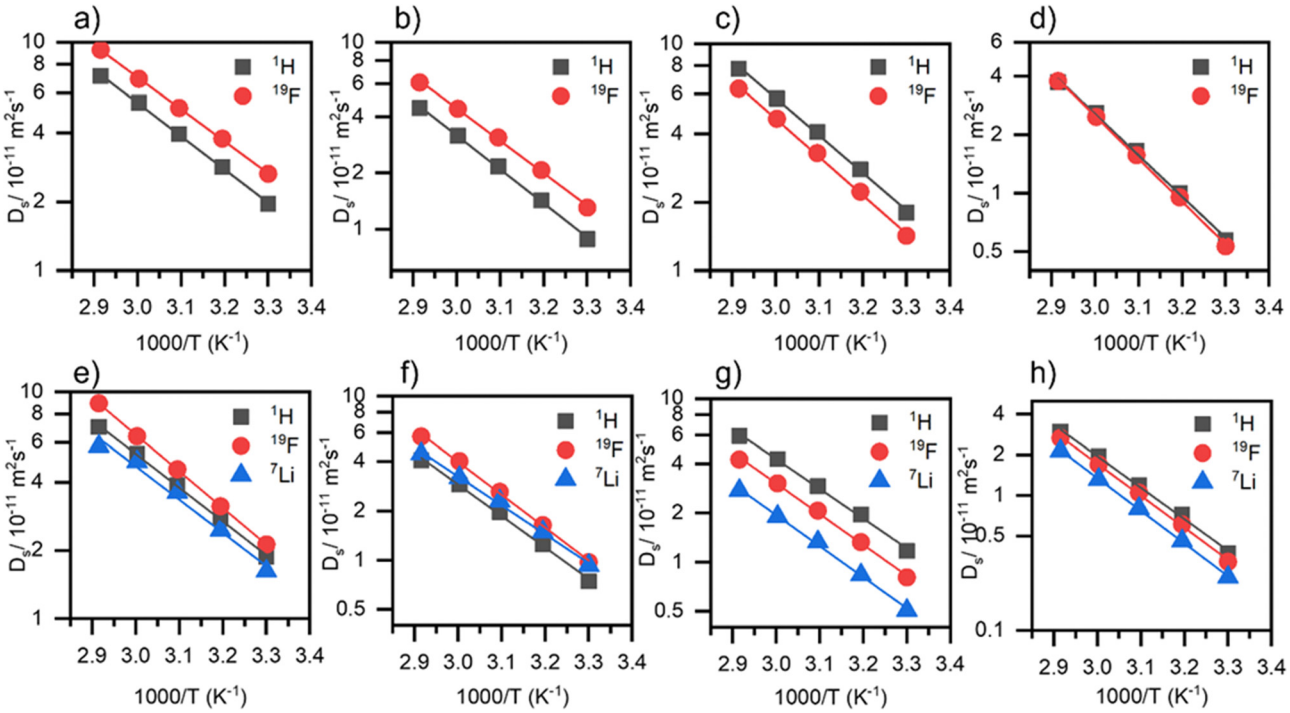

Fig. 6 Temperature dependent self-diffusion coefficients (^1H: IL cation, ^{19}F: anion, ^7Li: lithium cation) of neat ILs on top row in order (a) $[C_{1O1}mpip][FSI]$, (b) $[C_{1O1}mmor][FSI]$, (c) $[C_{1O1}mpip][TFSI]$, (d) $[C_{1O1}mmor][TFSI]$ and their electrolyte solutions directly below, in temperature range 30–70 °C. Errors are within the size of the data points.

Table 4 Activation energies of the self-diffusion coefficients for the ionic liquid cations (^{1}H), the common anion (^{19}F) and lithium cation (^{7}Li) for bulk ionic liquids and their electrolyte solutions. Weighted activation energies $E_{a,Ds(i)}$ are obtained by taking the stoichiometric coefficients of the anions in the mixtures into account. Values are obtained from Arrhenius fit in the T-range of 25–60 °C

Ionic liquid	$E_{a,Ds(1H)}$/ kJ mol^{-1}	$E_{a,Ds(19F)}$/ kJ mol^{-1}	$E_{a,Ds(7Li)}$/ kJ mol^{-1}	$E_{a,Ds(i)}$/ kJ mol^{-1}
[C$_{1O1}$mpip][FSI]	29	27	—	28
(LiFSI)$_{0.1}$([C$_{1O1}$mpip][FSI])$_{0.9}$	30	30	31	30
[C$_{1O1}$mmor][FSI]	35	35	—	35
(LiFSI)$_{0.1}$([C$_{1O1}$mmor][FSI])$_{0.9}$	39	40	38	39
[C$_{1O1}$mpip][TFSI]	33	34	—	34
(LiTFSI)$_{0.1}$([C$_{1O1}$mpip][TFSI])$_{0.9}$	37	38	38	38
[C$_{1O1}$mmor][TFSI]	43	44	—	43
(LiTFSI)$_{0.1}$([C$_{1O1}$mmor][TFSI])$_{0.9}$	47	48	48	48

$D_s(^{19}F)$ values of 1.8×10^{-11} and 1.4×10^{-11} m^2 s^{-1} respectively, at 30 °C so there is approximately a 35 and 43% decrease in diffusion coefficient for $D_s(^1H)$ and $D_s(^{19}F)$ respectively upon addition of Li^+, which are the largest decreases in diffusion coefficients observed across the four electrolyte systems. Despite these large decreases in diffusion coefficients observed for the cation and anion, lithium displays significantly lower diffusion, tentatively attributed to strong ion association with the anions.[56,57]

The activation energy for diffusion coefficients, $E_{a,Ds(i)}$, reveals the energy barrier for one ion to diffuse from one position to another and depends on local ion interactions.[58] Activation energies ($E_{a,Ds(i)}$) increase when changing the cation from $[C_{1O1}mpip]^+$ to $[C_{1O1}mmor]^+$ and changing the anion from $[FSI]^-$ to $[TFSI]^-$. Activation energies follow the trend $E_{a,Ds(i)} > E_{a,\eta} > E_{\Lambda imp}$ in all cases, which has been found for other ILs.[10] The ratio of $E_{\Lambda imp}/E_{a,\eta}$ relates to the exponential factor α from the Walden plot analysis.[42] Since $E_{\Lambda imp}/E_{a,\eta}$ is calculated to be below 1 in the systems presented here, it indicates that viscosity and molar conductivity do not show an ideal inverse relationship, which is discussed further in the ionicity section. It has been suggested by Green *et al.* that in the measurement of viscosity, shear flow may partially destroy some aggregates that form between ions, while NMR records diffusion of ions in a "static" environment where aggregates are preserved, yielding a higher activation energy for diffusion coefficients than for viscosity.[59]

Ionicity

The ionicity of the neat ILs and their electrolyte solutions was assessed with the Walden Plot approach, and the molar conductivity ratio approach.[60] A Walden plot allows a qualitative assessment of ionicity of ILs, by relating molar conductivity (Λ_{imp}) and fluidity (reciprocal viscosity, η^{-1}). Typically, there is an inverse relationship between viscosity, the resistivity to flow of the IL, and conductance, the mobility of ions carrying charge. However, lower viscosities do not always translate to higher conductivity, as seen with [C$_{1O1}$mpip][TFSI] and [C$_{1O1}$mmor][FSI]. This lack of a direct trend shows other factors intrinsic to these ILs are contributing to their properties, including degree of ion association/aggregate formation, which can be probed with the fractional Walden rule. The fractional Walden rule is presented in the following equation (eqn (3)):

$$\log \Lambda_{imp} = \log C + a \log \eta^{-1} \quad (3)$$

where α is an exponential factor used to describe the rate of increase of ion pairing over a specified temperature range, and C is the intercept. A calibration line which represents 0.01 M KCl solution is often referenced, where the ions are assumed to be fully dissociated and move independently in an electric field and so ionicity equals unity.[60] Fig. 7a and b shows the Walden plot for the ILs and their electrolyte solutions. In each case, the data lies close to the KCl line, and these ILs can be classified as "good ILs", having relatively high ionicity, according to Angell.[61] The degree of ionicity of the ILs can be approximated by the vertical deviation from the ideal KCl line (ΔW), where $\Delta W = 0$ would indicate full ion dissociation, and $\Delta W = 1$ indicates only 10% ion dissociation (10% ionicity line is shown in Fig. 7). The ΔW values (Table S6, ESI†) increase with temperature, indicating ion pairing as temperature increases, and lie between 0.15–0.27 over the temperature range analysed, with the general trend from most dissociated to least dissociated (*i.e.* lowest to highest ΔW values) in the order [C$_{1O1}$mpip][FSI] > [C$_{1O1}$mmor][TFSI] ≈ [C$_{1O1}$mmor][FSI] > [C$_{1O1}$mpip][TFSI]. No clear trend is observed for ΔW values as the deviations from the KCl line are all quite small and similar to each other. Similar values are observed for other ILs such as [N$_{11,1O1}$][TFSI] and [C$_{1O1}$mpyr][TFSI], which have ΔW values at 30 °C of 0.21 and 0.26 respectively.[13,62]

Upon addition of Li–salt the ΔW values increase to 0.21–0.32 due to Li^+ interacting with anions that form ion pairs and aggregates. As the temperature increases, ΔW increases more for the TFSI-based electrolytes, indicating a higher degree of ion association or Li^+ aggregates forming at higher temperatures than for FSI-based electrolytes. This temperature trend of increasing ΔW with temperature is consistent with that of other ILs.[63]

A second approach to analysing the degree of ion association in ILs is the ionicity approach estimated by the molar conductivity.[60] The Nernst–Einstein equation (eqn (4)) is used to estimate molar conductivity (Λ_{NMR}) from the PFG-NMR diffusion coefficients:

$$\Lambda_{NMR} = \frac{N_A e^2 (D^+ + D^-)}{kT} = \frac{F^2 (D^+ + D^-)}{RT} \quad (4)$$

where N_A is the Avogadro number, e is the electric charge on each ionic carrier (1.602×10^{-19} C), k is the Boltzmann constant, T is the absolute temperature (K), F is the Faraday constant, and R is the universal gas constant. The temperature dependant Λ_{NMR} values calculated from eqn (4), and the experimental molar conductivity (Λ_{imp}) and Λ_{NMR} are shown in Tables S7 and S8 (ESI†), respectively. Across the entire temperature range, the Λ_{NMR} values are higher than Λ_{imp} for all ILs because molar conductivity calculated from the NMR data using the Nernst–Einstein equation assumes all diffusing species, both charged and paired ions, contribute to the molar conductivity. In contrast, molar conductivity calculated by

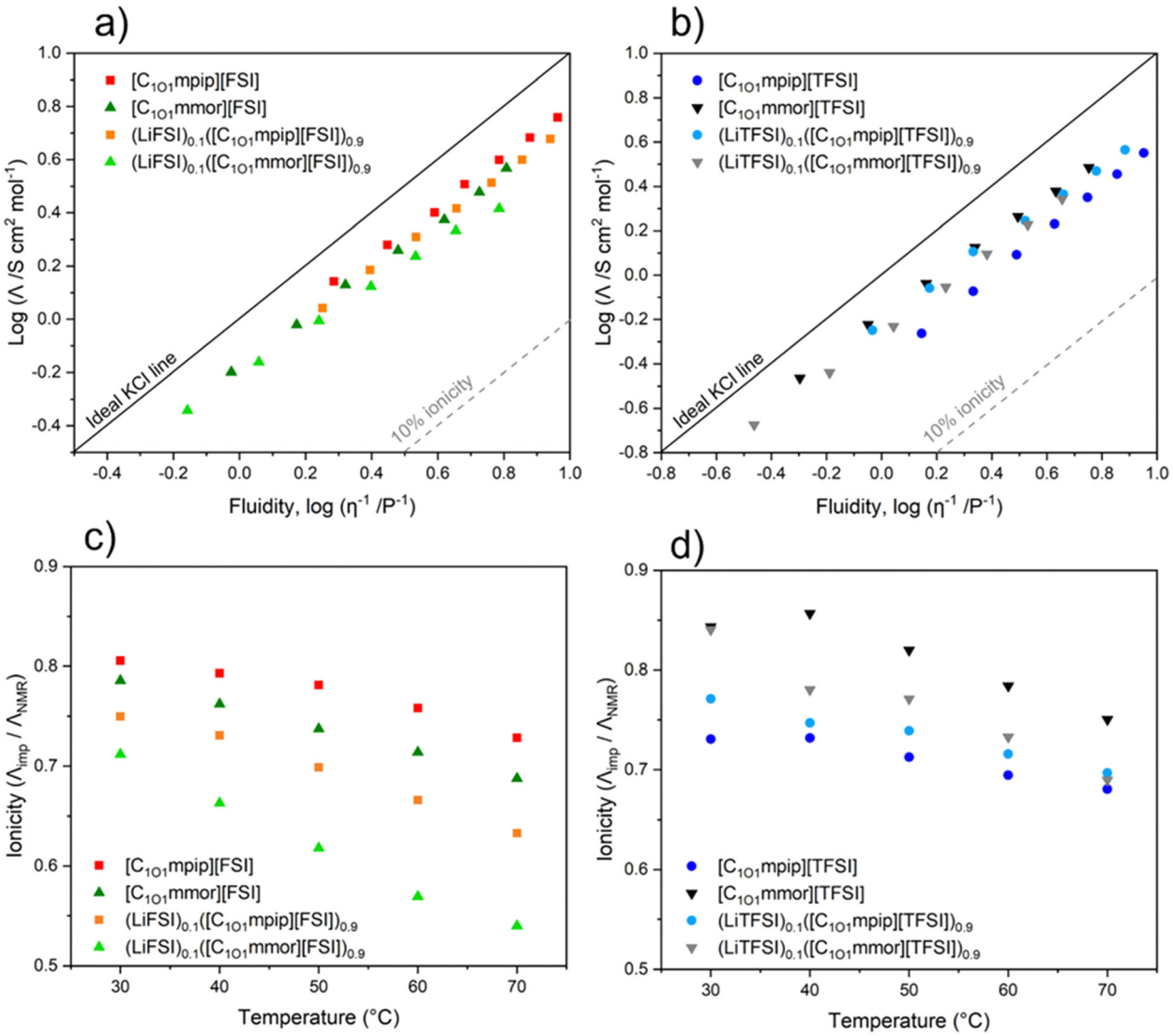

Fig. 7 Walden plot for (a) FSI-based ILs and their electrolyte solutions and (b) TFSI-based ILs and their electrolyte solutions, where Λ is molar conductivity calculated from experimental impedance data and η^{-1} is fluidity, and temperature-dependant ionicity I_{HR} of (c) FSI-based ILs and their electrolytes and (d) TFSI-based ILs and their electrolytes. Errors were calculated at <4% for all ionicity measurements.

electrochemical impedance spectroscopy (Λ_{imp}) measures the migration of only charged species (not neutral aggregates) in an electric field. Therefore, the ratio of Λ_{imp} and Λ_{NMR} (I_{HR}, the inverse of the Haven ratio) represents the proportion of ions that contribute to ion conduction from all diffusing species and is interpreted as the amount of 'free ions' in the IL.[60]

A plot of ionicity ($\Lambda_{imp}/\Lambda_{NMR}$) *vs.* temperature is shown in Fig. 7c and d. The I_{HR} values show a narrow distribution of ionicity values between 0.84 and 0.73 at 30 °C, which decrease with temperature due to increased ion pairing or aggregate formation at higher temperatures, with the general trend from most dissociated to least dissociated (*i.e.* highest to lowest ionicity) in the order [C$_{1O1}$mmor][TFSI] > [C$_{1O1}$mpip][FSI] > [C$_{1O1}$mmor][FSI] > [C$_{1O1}$mpip][TFSI]. The trend from the Walden analysis was slightly different, likely reflecting experimental uncertainty, giving [C$_{1O1}$mpip][FSI] > [C$_{1O1}$mmor][TFSI] ≈ [C$_{1O1}$mmor][FSI] > [C$_{1O1}$mpip][TFSI].

Both [C$_{1O1}$mpip][TFSI] and [C$_{1O1}$mmor][FSI] have comparable conductivities, despite the piperidinium IL having a lower viscosity at 30 °C (91 mPa s compared to 139 mPa s for [C$_{1O1}$mmor][FSI]). Both the Walden Plot and I_{HR} indicate that this is due to [C$_{1O1}$mpip][TFSI] having a lower number of free charge carriers due to more ion association compared to [C$_{1O1}$mmor][FSI], as the TFSI anions have a lower tendency to dissociate than FSI anions. At 30 °C, this is confirmed by [C$_{1O1}$mmor][FSI] having a lower ΔW value and higher I_{HR} ($\Lambda_{imp}/\Lambda_{NMR}$) value than [C$_{1O1}$mpip][TFSI] ($\Delta W$ = 0.17 and 0.21, and I_{HR} = 0.79 and 0.73, respectively).

All the ILs lie in a narrow distribution range of ionicity and show a similar picture from each approach. [C$_{1O1}$mpip][TFSI] has the lowest degree of ion dissociation, followed by [C$_{1O1}$mmor][FSI]. [C$_{1O1}$mpip][FSI] and [C$_{1O1}$mmor][TFSI] have the highest degree of ion association. Usually, FSI-based ILs tend to have higher I_{HR} values compared to TFSI-based ILs with

the same cation,[64] and this trend is observed for $[C_{1O1}mpip]^+$ based ILs but not $[C_{1O1}mmor]^+$ based ILs. $[C_{1O1}mmor][TFSI]$ has a higher I_{HR} value (more dissociation) compared to $[C_{1O1}mpip][TFSI]$, but upon addition of LiTFSI, the electrolytes have similar I_{HR} values, suggesting potentially more $[C_{1O1}mmor]^+$ cations are interacting with Li^+. For FSI-based systems, upon addition of Li–salt, both electrolytes result in lower ionicity compared to the neat ILs. At higher temperatures, ionicity decreases for all systems. A possible reason for this complex behaviour may be a change in transport mechanism.[65]

Electrochemical stability windows

The electrochemical stability window (ΔE) defines the potential range in which the IL is stable and does not undergo oxidation or reduction. Wide ΔE's can result in more oxidising cathodes being employed, unlocking higher power density in batteries. The ΔE of the ILs were measured using cyclic voltammetry (CV), as an initial assessment to their suitability as electrolytes, at a 3 mm diameter glassy carbon electrode. The onset potentials of reductive and oxidative decomposition (E_a and E_c, respectively) of the ILs are defined using a cut-off current density of ± 0.1 mA cm^{-2}. The ΔE is defined as the difference between the anodic and cathodic potential limits ($\Delta E = E_a - E_c$) The electrochemical windows of the ILs are presented in Fig. S6 (ESI†) and the potential values are summarised in Table 5. An internal ferrocene redox couple was used to normalise the reference potential *vs.* the Fc/Fc^+ redox potential.

The data presented in Table 5 shows evident trends in the electrochemical stabilities of these ILs. The CVs of the four ILs show the onset of electrolyte decomposition by reduction and oxidation in the regions of -4.0 to -2.7) V *vs.* Fc/Fc^+ and 2.0 to 2.3 V *vs.* Fc/Fc^+. The $TFSI^-$ anion is more electrochemically stable than the FSI^- anion, as reported elsewhere,[66] and as such the TFSI-based ILs lead to higher ΔE compared to FSI-based ILs. $[C_{1O1}mmor][TFSI]$ has the lowest reductive potential at -3.2 V, and the widest ΔE, at 5.5 V. Both $[C_{1O1}mmor][FSI]$ and $[C_{1O1}mpip][TFSI]$ also have electrochemical stability windows above 5 V, allowing the use of high voltage cathode materials such as olivine structured $LiMPO_4$ materials.[67] The ΔE for both morpholinium-based ILs are significantly higher than $[C_4mmor][TFSI]$ (4.5 V)[68] and $[C_4mmor][FSI]$ (3 V).[69] The higher oxidative stability of $[C_{1O1}mmor][FSI]$ compared to $[C_{1O1}mpip][FSI]$ is somewhat surprising considering the introduction of oxygen to the cation chain decreases the ΔE as observed with $[C_3mpip][TFSI]$ (5.9 V) and $[C_3mpip][FSI]$ (5.6 V),[46] compared with $[C_{1O1}mpip][TFSI]$ (5.2 V) and $[C_{1O1}mpip][FSI]$ (4.7 V) here, due to a decrease in both cathodic and anodic limits upon ether-functionalisation. However, the trend of a wider ΔE for morpholinium-based ILs has previously been observed with the ethoxyethyl chain, where $[C_{2O2}mmor][FSI]$ has a wider electrochemical window than $[C_{2O2}mpip][FSI]$ (4.6 and 4.0 V, respectively).[70] Overall, all four ILs possess sufficiently wide electrochemical stability for future investigation into Li electrochemical applications.

Table 5 Onset potentials of cathodic (E_c) and anodic (E_a) decomposition and the ILs electrochemical stability windows, ΔE, as determined by cyclic voltammetry at a GC working electrode, at 25 °C

Ionic liquid	E_c (V *vs.* Fc/Fc^+)	E_a (V *vs.* Fc/Fc^+)	ΔE (V)
$[C_{1O1}mpip][FSI]$	−2.7	2.0	4.7
$[C_{1O1}mmor][FSI]$	−2.9	2.5	5.4
$[C_{1O1}mpip][TFSI]$	−3.1	2.1	5.2
$[C_{1O1}mmor][TFSI]$	−3.2	2.3	5.5

Interaction of Li^+ and TFSI counter anion in ionic liquid

Weakening Li^+–solvent interactions is beneficial for improving Li^+ diffusion and enhancing rate performance in batteries.[12] Therefore, low Li–anion solvation numbers are desirable. FTIR spectroscopy can elucidate the presence of *cis*- and *trans*-conformers of the TFSI anion, where weak interactions between cations and anions favour *trans*-TFSI.[71]

The IR spectra of $[C_{1O1}mpip][TFSI]$ and $[C_{1O1}mmor][TFSI]$ and their electrolyte solutions were measured as a function of temperature between 30 and 90 °C, in the frequency range between 580 and 680 cm^{-1}, where the peak present is a contribution of the two conformers which can be clearly identified,[39,72,73] and are reported in Fig. S7 (ESI†). Deconvolution of these peaks (an example of the deconvoluted peaks is presented in Fig. S8, ESI†) can be used to calculate the enthalpy difference (ΔH) between *cis*- and *trans*-TFSI conformers in each IL, with a higher ΔH indicating a higher concentration of the more stable *trans*-TFSI.[39] A higher ΔH was observed in $[C_{1O1}mmor][TFSI]$ compared to $[C_{1O1}mpip][TFSI]$ and ΔH decreased upon addition of LiTFSI in both electrolytes. A higher concentration of *trans*-TFSI indicates weaker interactions between the cation and anion and therefore more fragile glass behaviour. Weak cation and anion interactions in the electrolyte systems are advantageous for Li^+ solvation and Li^+ diffusion. Further discussion of the IR data is in the ESI.† However, we found Raman analysis to be more insightful for quantitative comparison of the lithium coordination in the new IL electrolytes and thus this approach is discussed in more detail below.

Raman spectroscopy was used to investigate the Li^+ coordination to the anions in the bulk electrolyte. When Li–salts are dissolved into a TFSI-based IL, Li^+ coordinates to the oxygen atoms in the anion by Coulombic force, to form $[Li(TFSI)_n]^{1-n}$ complexes. The higher the solvation number (n), the slower the diffusion of the complex, which leads to drawbacks such as low lithium transport numbers and has a large influence on the charge–discharge properties of batteries. When n is above 1, the overall charge of the Li^+ complex is negative. It has previously been found that oxygens on the chain of a cation play a key role in weakening the Li–anion interactions and lowering the solvation number, due to an attractive force generated between the electronegative oxygen atoms on the cation and the Li^+, and that multiple oxygens on the cation chain lead to further increase the Li–cation interaction and thus further weaken the interactions between the Li^+ and the anion.[12] The effect of having an oxygen on the ring *vs.* the chain has not yet been explored to understand if there is a benefit to one position over the other.

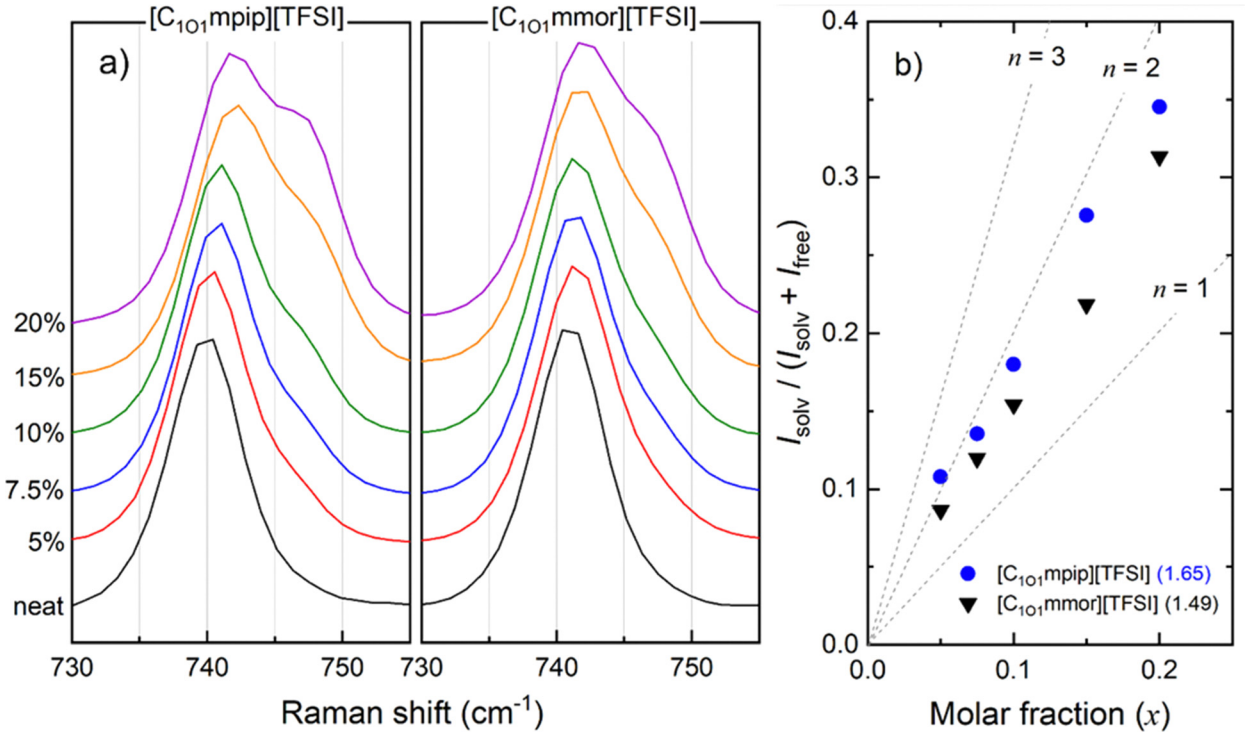

Fig. 8 (a) Raman spectra of $(LiTFSI)_x([C_{1O1}mpip][TFSI])_{1-x}$ (left) and $(LiTFSI)_x([C_{1O1}mmor][TFSI])_{1-x}$ (right) electrolyte solutions from 730 to 755 cm^{-1}. where x is 0 (black), 0.05 (red), 0.075 (blue), 0.10 (green), 0.15 (orange), and 0.2 (purple) and (b) plot of $I_{solv}/(I_{free} + I_{solv})$ as a function of $(LiTFSI)_x([C_{1O1}mpip][TFSI])_{1-x}$ and $(LiTFSI)_x([C_{1O1}mmor][TFSI])_{1-x}$ where the slope represents the average solvation number. The grey dashed reference lines represent the slope when the average solvation number (n) =1, 2 or 3.

The bending vibration of the CF_3 group coupled with a stretching vibration of S–N–S in the TFSI anion appears at around 742 cm^{-1}.[16] When TFSI anions are coordinated to Li-ions, known as contact ion pairs, the band is shifted to 744–747 cm^{-1}, or further still in the case of aggregates, where an anion is coordinated to two or more Li^+ cations, to 747–750 cm^{-1}. Aggregates are usually formed at high Li–salt concentrations. Here, two peaks have been assigned, as either "free" anions (or very weakly coordinated anions) at approximately 742 cm^{-1} or "solvated" anions, which may include both contact ion pairs and aggregates, at approximately 748 cm^{-1}. Furthermore, due to both *trans*- and *cis*-TFSI anions being present, four oxygens per TFSI anion that can coordinate to Li^+, and TFSI anions undergoing rapid conformational dynamic exchange during measurements,[74] the Raman peaks analysed are broadened. Therefore, the analysis herein is more qualitative than quantitative, but deconvolution of peaks has been followed by reported methods, and as such we have compared data to other similar systems following the same method.[75,76]

For analysis of the spectral results shown in Fig. 8a, the spectral regions were fitted with a fixed 40 : 60 Gaussian: Lorentzian ratio profile (Fig. S9, ESI†), to obtain the integrals of the peaks of the 'free' anion and coordinated species. The average solvation number is calculated by a method reported by Lassègues and Balducci *et al.*[75,76] The slope of a plot of the ratio of solvated anions to both solvated and free anions (eqn (5)) *vs.* molar fraction of LiTFSI determines the average solvation number, shown in Fig. 8b.

$$n = \frac{I_{742}}{I_{742} + I_{748}} = \frac{[I_{solv}]}{[I_{solv}] + [I_{free}]} \quad (5)$$

In both ILs, the band at 742 cm^{-1} is larger than 748 cm^{-1}, indicating there is always a larger concentration of free TFSI anions than coordinated across the whole Li–salt concentration range studied (LiTFSI molar fractions = 0.05, 0.075, 0.1, 0.15 and 0.2). At 20 mol% LiTFSI, $[C_{1O1}mpip][TFSI]$ has resulted in a lower solvation number of 1.65 compared to the cation with a longer ether-chain *N*-methoxybutyl-*N*-methylpiperidinium $[C_{1O4}mpip][TFSI]$, which has solvation number of 1.76 at the same LiTFSI concentration range.[12] More aggregation in the cation with longer side chain can lead to a higher solvation number. When there are two oxygens on the cation, the formation of $[Li(TFSI)_n]^{1-n}$ complexes is further suppressed. $(LiTFSI)_{0.2}([C_{1O1}mmor][TFSI])_{0.8}$ has a solvation number of 1.49, which is lower than when two oxygens are located on the chain in the case of $(LiTFSI)_{0.2}([C_{1O2O1}mpip][TFSI])_{0.8}$, which has a solvation number of 1.56.

The lower solvation number for $[C_{1O1}mmor][TFSI]$ indicates fewer $[TFSI]^-$ anions coordinate to each Li^+ ion, meaning the Li^+ in $[C_{1O1}mmor][TFSI]$ is less constrained by interactions with anions, and the overall smaller Li-complex is able to diffuse faster through the liquid. To confirm this, a reciprocal viscosity (fluidity) *vs.* Li^+ diffusion coefficient plot is shown in Fig. S10 (ESI†) to compare Li^+ solvation in each system. At any given

fluidity, the Li^+ diffusion coefficient is fastest to slowest in the different IL-based electrolytes in the order $[C_{1O1}mmor][FSI] > [C_{1O1}mpip][FSI] > [C_{1O1}mmor][TFSI] > [C_{1O1}mpip][TFSI]$. Assuming that Li^+ moves as a cluster rather than hopping between ions by rearrangement of the solvation sphere or exchange of coordination environment,[77] it can be concluded that the coordination environment in the $[C_{1O1}mmor]^+$ electrolyte has a beneficial impact on Li^+ diffusion as the Li^+ is able to diffuse faster in this IL than in the $[C_{1O1}mpip]^+$ system even at the same viscosity. The second oxygen in the $[C_{1O1}mmor]^+$ cation is therefore concluded to be important in weakening interactions between Li^+ and anions, but also plays a role in decreasing the concentration of *cis*-$[TFSI]^-$ anions present in the electrolyte, as observed with FTIR, which preferably coordinate to Li^+ ions.

Conclusions

Three new ILs were synthesised, as well as $[C_{1O1}mpip][TFSI]$ at a higher yield than previously reported. Two cations were synthesised and paired with TFSI and FSI anions to study the effect of the position and number of oxygen atoms within the cation with each anion on the structure–property relationships of the neat ILs and their lithium electrolyte compositions, including ionicity by Walden plot method and comparisons of molar conductivity calculated by EIS and PFG-NMR.

The thermal behaviour shows the effect of anion where TFSI-based ILs only show a T_g whereas FSI-based ILs had melting points which were suppressed upon lithiation, enabling a wide working temperature range as liquid electrolytes. All the electrolyte compositions resulted in low T_g values of below −64 °C. The morpholinium ILs were found to have higher densities and viscosities compared to the corresponding piperidinium ILs, while the addition of Li–salts further increased these values.

$[C_{1O1}mpip][FSI]$ showed particularly promising properties, such as a viscosity value of 51.8 mPa s and conductivity of 5.9×10^{-3} S cm^{-1} at 30 °C, and high ionicity value of 0.81 at 30 °C, indicating a high degree of ion dissociation. These values were almost retained upon LiFSI addition, resulting in a conductivity of 5.0×10^{-3} S cm^{-1} and the fastest Li^+ diffusion at 1.6×10^{-11} cm^2 s^{-1} at 30 °C. However, when comparing Li^+ diffusion to fluidity (η^{-1}), at a given fluidity the $[C_{1O1}mmor][FSI]$ results in the fastest Li^+ diffusion, with the morpholinium-based electrolytes resulting in faster Li^+ diffusion in both anion systems.

All of the neat ionic liquids, except for $[C_{1O1}mpip][FSI]$ display electrochemical stability windows above 5 V, while $[C_{1O1}mpip][FSI]$ has an electrochemical stability window of 4.7 V. Thus, an initial investigation shows sufficient electrochemical stability to support extended electrochemical studies on the development of these new ionic liquids for battery applications.

The solvation environment of Li-ions in the respective TFSI-based electrolytes was analysed with Raman spectroscopy and revealed the methoxymethyl chain functionality is beneficial to lowering the average solvation number of TFSI anions per Li-ion, which is expected to be advantageous for their use as electrolytes in lithium batteries. Moreover, the second oxygen in the morpholinium cation lowers the average solvation number further from 1.65 for $(LiTFSI)_{0.2}([C_{1O1}mpip][TFSI])_{0.8}$ to 1.49 for $(LiTFSI)_{0.2}([C_{1O1}mmor][TFSI])_{0.8}$, which contributes to a higher relative diffusion for Li^+ observed in PFG-NMR.

In conclusion, novel ether-functionalised piperidinium and morpholinium-based ionic liquids including their corresponding electrolyte systems with LiFSI and LiTFSI demonstrate a range of advantages over alkyl equivalent ILs and cations with longer ether-functionalised chains, such as reduced viscosity and weakened Li–anion interactions. Incorporating short ether-functionalised chains on to the cation is an approach that points towards high performance IL-based electrolytes for lithium metal batteries as a viable safe alternative to the traditional carbonate-based solvents. Future work will include electrochemical study on Li-transference, Li deposition and stripping behaviour, and cell cycling under realistic conditions. This work has the potential to be extended to various other rechargeable battery systems, for instance to increase target ion transport to other alkali metal batteries such as sodium or potassium.

Conflicts of interest

There are no conflicts to declare.

Acknowledgements

This work was supported by funding received from the Australian Research Council (ARC) through the ARC Training Centre in Future Energy Storage Technologies IC180100049 (StorEnergy). The authors thank Dr Colin S. M. Kang for his valuable input.

References

1 H. Tokuda, K. Hayamizu, K. Ishii, M. A. B. H. Susan and M. Watanabe, Physicochemical Properties and Structures of Room Temperature Ionic Liquids. 2. Variation of Alkyl Chain Length in Imidazolium Cation, *J. Phys. Chem. B*, 2005, **109**, 6103–6110.

2 S. P. Ong, O. Andreussi, Y. Wu, N. Marzari and G. Ceder, Electrochemical windows of room-temperature ionic liquids from molecular dynamics and density functional theory calculations, *Chem. Mater.*, 2011, **23**, 2979–2986.

3 M. Hasanpoor, D. Saurel, R. C. Barreno, K. Fraysse, M. Echeverría, M. Jáuregui, F. Bonilla, G. W. Greene, R. Kerr, M. Forsyth and P. C. Howlett, Morphological Evolution and Solid–Electrolyte Interphase Formation on $LiNi_{0.6}Mn_{0.2}Co_{0.2}O_2$ Cathodes Using Highly Concentrated Ionic Liquid Electrolytes, *ACS Appl. Mater. Interfaces*, 2022, **14**, 13196–13205.

4 L. Grande, J. Von Zamory, S. L. Koch, J. Kalhoff, E. Paillard and S. Passerini, Homogeneous Lithium Electrodeposition with Pyrrolidinium-Based Ionic Liquid Electrolytes, *ACS Appl. Mater. Interfaces*, 2015, **7**, 5950–5958.

5 S. Jurng, Z. L. Brown, J. Kim and B. L. Lucht, Effect of electrolyte on the nanostructure of the solid electrolyte interphase (SEI) and performance of lithium metal anodes, *Energy Environ. Sci.*, 2018, **11**, 2600–2608.

6 K. Periyapperuma, E. Arca, S. Harvey, T. Pathirana, C. Ban, A. Burrell, C. Pozo-Gonzalo and P. C. Howlett, High Current Cycling in a Superconcentrated Ionic Liquid Electrolyte to Promote Uniform Li Morphology and a Uniform LiF-Rich Solid Electrolyte Interphase, *ACS Appl. Mater. Interfaces*, 2020, **12**, 42236–42247.

7 W. Zhang, Q. Ma, X. Liu, S. Yang and F. Yu, Novel piperidinium-based ionic liquid as electrolyte additive for high voltage lithium-ion batteries, *RSC Adv.*, 2021, **11**, 15091–15098.

8 S. Xiong, K. Xie, E. Blomberg, P. Jacobsson and A. Matic, Analysis of the solid electrolyte interphase formed with an ionic liquid electrolyte for lithium-sulfur batteries, *J. Power Sources*, 2014, **252**, 150–155.

9 A. R. Neale, S. Murphy, P. Goodrich, C. Hardacre and J. Jacquemin, Thermophysical and Electrochemical Properties of Ethereal Functionalised Cyclic Alkylammonium-based Ionic Liquids as Potential Electrolytes for Electrochemical Applications, *ChemPhysChem*, 2017, **18**, 2040–2057.

10 D. Rauber, A. Hofmann, F. Philippi, C. W. M. Kay, T. Zinkevich, T. Hanemann and R. Hempelmann, Structure–Property Relation of Trimethyl Ammonium Ionic Liquids for Battery Applications, *Appl. Sci.*, 2021, **11**, 5679–5702.

11 K. Yoshii, T. Uto, T. Onishi, D. Kosuga, N. Tachikawa and Y. Katayama, Ether-functionalized Pyrrolidinium-based Room Temperature Ionic Liquids: Physicochemical Properties, Molecular Dynamics, and the Li ion Coordination Environment, *ChemPhysChem*, 2021, **22**, 1–12.

12 M. Shimizu, K. Yamaguchi, H. Usui, N. Ieuji, T. Yamashita, T. Komura, Y. Domi, T. Nokami, T. Itoh and H. Sakaguchi, Piperidinium-Based Ionic Liquids as an Electrolyte Solvent for Li-Ion Batteries: Effect of Number and Position of Oxygen Atom in Cation Side Chain on Electrolyte Property, *J. Electrochem. Soc.*, 2020, **167**, 070516–070520.

13 A. Warrington, C. S. M. Kang, C. Forsyth, C. M. Doherty, D. Acharya, L. A. O'Dell, N. Sirigiri, J. W. Boyle, O. E. Hutt, M. Forsyth and J. M. Pringle, Thermal, structural and dynamic properties of ionic liquids and organic ionic plastic crystals with a small ether-functionalised cation, *Mater. Chem. Front.*, 2022, **6**, 1437–1455.

14 S. Seki, S. Tsuzuki, K. Hayamizu, N. Serizawa, S. Ono, K. Takei, H. Doi and Y. Umebayashi, Static and transport properties of alkyltrimethylammonium cation-based room-temperature ionic liquids, *J. Phys. Chem. B*, 2014, **118**, 4590–4599.

15 M. Shimizu, H. Usui, K. Matsumoto, T. Nokami, T. Itoh and H. Sakaguchi, Effect of Cation Structure of Ionic Liquids on Anode Properties of Si Electrodes for LIB, *J. Electrochem. Soc.*, 2014, **161**, A1765–A1771.

16 Y. Umebayashi, T. Mitsugi, S. Fukuda, T. Fujimori, K. Fujii, R. Kanzaki, M. Takeuchi and S. I. Ishiguro, Lithium ion solvation in room-temperature ionic liquids involving bis(trifluoromethanesulfonyl) imide anion studied by Raman spectroscopy and DFT calculations, *J. Phys. Chem. B*, 2007, **111**, 13028–13032.

17 M. Shimizu, H. Usui and H. Sakaguchi, Functional ionic liquids for enhancement of Li-ion transfer: The effect of cation structure on the charge–discharge performance of the $Li_4Ti_5O_{12}$ electrode, *Phys. Chem. Chem. Phys.*, 2016, **18**, 5139–5147.

18 K. Yamaguchi, H. Usui, Y. Domi, H. Nishida, T. Komura, T. Nokami, T. Itoh and H. Sakaguchi, Electrochemical performance of Sn_4P_3 negative electrode for Na-ion batteries in ether-substituted ionic liquid electrolyte, *J. Electroanal. Chem.*, 2019, **845**, 66–71.

19 Q. Huang, Y. Y. Lee and B. Gurkan, Pyrrolidinium Ionic Liquid Electrolyte with Bis(trifluoromethylsulfonyl)imide and Bis(fluorosulfonyl)imide Anions: Lithium Solvation and Mobility, and Performance in Lithium Metal-Lithium Iron Phosphate Batteries, *Ind. Eng. Chem. Res.*, 2019, **58**, 22587–22597.

20 Q. Huang, T. C. Lourenco, L. T. Costa, Y. Zhang, E. J. Maginn and B. Gurkan, Solvation structure and dynamics of Li^+ in ternary ionic liquid– Lithium salt electrolytes, *J. Phys. Chem. B*, 2019, **123**, 516–527.

21 P.-A. Martin, F. Chen, M. Forsyth, M. Deschamps and L. A. O'Dell, Correlating Intermolecular Cross-Relaxation Rates with Distances and Coordination Numbers in Ionic Liquids, *J. Phys. Chem. Lett.*, 2018, **9**, 7072–7078.

22 H. Yoon, S. Shin, S. Park and M. W. Shin, Low-viscosity quaternary ammonium-based ionic liquid electrolytes for lithium air batteries, *J. Mol. Liq.*, 2022, **359**, 119352–119358.

23 S. Horiuchi, M. Yoshizawa-Fujita, Y. Takeoka and M. Rikukawa, Physicochemical and electrochemical properties of *N*-methyl-*N*-methoxymethylpyrrolidinium bis(fluorosulfonyl)amide and its lithium salt composites, *J. Power Sources*, 2016, **325**, 637–640.

24 J. Chapman Varela, K. Sankar, A. Hino, X. Lin, W. S. Chang, D. Coker and M. Grinstaff, Piperidinium ionic liquids as electrolyte solvents for sustained high temperature supercapacitor operation, *Chem. Commun.*, 2018, **54**, 5590–5593.

25 J. E. Tanner and E. O. Stejskal, Restricted self-diffusion of protons in colloidal systems by the pulsed-gradient, spin-echo method, *J. Chem. Phys.*, 1968, **49**, 1768–1777.

26 E. O. Stejskal and J. E. Tanner, Spin diffusion measurements: Spin echoes in the presence of a time-dependent field gradient, *J. Chem. Phys.*, 1965, **42**, 288–292.

27 W. Xu, E. I. Cooper and C. A. Angell, Ionic liquids: Ion mobilities, glass temperatures, and fragilities, *J. Phys. Chem. B*, 2003, **107**, 6170–6178.

28 C. A. Angell, Formation of glasses from liquids and biopolymers, *Science*, 1995, **267**, 1924–1935.

29 M. J. Monteiro, F. F. C. Bazito, L. J. A. Siqueira, M. C. C. Ribeiro and R. M. Torresi, Transport coefficients,

Raman spectroscopy, and computer simulation of lithium salt solutions in an ionic liquid, *J. Phys. Chem. B*, 2008, **112**, 2102–2109.

30 X. Wang, Y. Chi and T. Mu, A review on the transport properties of ionic liquids, *J. Mol. Liq.*, 2014, **193**, 262–266.

31 E. Gómez, N. Calvar and Á. Domínguez, in *Ionic Liquids – Current State of the Art*, ed. S. Handy, InTech Open, 2015, pp. 202–204.

32 M. A. Navarra, K. Fujimura, M. Sgambetterra, A. Tsurumaki, S. Panero, N. Nakamura, H. Ohno and B. Scrosati, New Ether-functionalized Morpholinium- and Piperidinium-based Ionic Liquids as Electrolyte Components in Lithium and Lithium–Ion Batteries, *ChemSusChem*, 2017, **10**, 2496–2504.

33 M. Montanino, M. Carewska, F. Alessandrini, S. Passerini and G. B. Appetecchi, The role of the cation aliphatic side chain length in piperidinium bis(trifluoromethansulfonyl)imide ionic liquids, *Electrochim. Acta*, 2011, **57**, 153–159.

34 J. Kim, R. P. Singh and J. M. Shreeve, Low Melting Inorganic Salts of Alkyl-, Fluoroalkyl-, Alkyl Ether-, and Fluoroalkyl Ether-Substituted Oxazolidine and Morpholine, *Inorg. Chem.*, 2004, **43**, 2960–2966.

35 C. Liu, X. Ma, F. Xu, L. Zheng, H. Zhang, W. Feng, X. Huang, M. Armand, J. Nie, H. Chen and Z. Zhou, Ionic liquid electrolyte of lithium bis(fluorosulfonyl)imide/*N*-methyl-*N*-propylpiperidinium bis(fluorosulfonyl)imide for Li/natural graphite cells: Effect of concentration of lithium salt on the physicochemical and electrochemical properties, *Electrochim. Acta*, 2014, **149**, 370–385.

36 M. Galiński, A. Lewandowski and I. Stepniak, Ionic liquids as electrolytes, *Electrochim. Acta*, 2006, **51**, 5567–5580.

37 S. Choi, K. Kim, J. Cha, H. Lee, J. S. Oh and B. Lee, Thermal and electrochemical properties of ionic liquids based on *N*-methyl-*N*-alkyl morpholinium cations, *Korean J. Chem. Eng.*, 2006, **23**, 795–799.

38 Z. Bin Zhou, H. Matsumoto and K. Tatsumi, Cyclic quaternary ammonium ionic liquids with perfluoroalkyltrifluoroborates: Synthesis, characterization, and properties, *Chem. – Eur. J.*, 2006, **12**, 2196–2212.

39 A. Tsurumaki, F. Trequattrini, O. Palumbo, S. Panero, A. Paolone and M. A. Navarra, The effect of ether-functionalisation in ionic liquids analysed by DFT calculation, infrared spectra, and Kamlet-Taft parameters, *Phys. Chem. Chem. Phys.*, 2018, **20**, 7989–7997.

40 S. Seki, N. Serizawa, S. Ono, K. Takei, K. Hayamizu, S. Tsuzuki and Y. Umebayashi, Densities, Viscosities, and Refractive Indices of Binary Room-Temperature Ionic Liquids with Common Cations/Anions, *J. Chem. Eng. Data*, 2019, **64**, 433–441.

41 I. Bandrés, R. Alcalde, C. Lafuente, M. Atilhan and S. Aparicio, On the viscosity of pyridinium based ionic liquids: An experimental and computational study, *J. Phys. Chem. B*, 2011, **115**, 12499–12513.

42 C. Schreiner, S. Zugmann, R. Hartl and H. J. Gores, Temperature dependence of viscosity and specific conductivity of fluoroborate-based ionic liquids in light of the fractional Walden rule and Angell's fragility concept, *J. Chem. Eng. Data*, 2010, **55**, 4372–4377.

43 M. Hilder, M. Gras, C. R. Pope, M. Kar, D. R. Macfarlane, M. Forsyth and L. A. O'Dell, Effect of mixed anions on the physicochemical properties of a sodium containing alkoxyammonium ionic liquid electrolyte, *Phys. Chem. Chem. Phys.*, 2017, **19**, 17461–17468.

44 P. Sippel, P. Lunkenheimer, S. Krohns, E. Thoms and A. Loidl, Importance of liquid fragility for energy applications of ionic liquids, *Sci. Rep.*, 2015, **5**, 13922–13929.

45 M. Kerner, N. Plylahan, J. Scheers and P. Johansson, Ionic liquid based lithium battery electrolytes: fundamental benefits of utilising both TFSI and FSI anions?, *Phys. Chem. Chem. Phys.*, 2015, **17**, 19569–19581.

46 H. Matsumoto, H. Sakaebe, K. Tatsumi, M. Kikuta, E. Ishiko and M. Kono, Fast cycling of Li/$LiCoO_2$ cell with low-viscosity ionic liquids based on bis(fluorosulfonyl)imide $[FSI]^-$, *J. Power Sources*, 2006, **160**, 1308–1313.

47 M. H. Ibrahim, M. Hayyan, M. A. Hashim, A. Hayyan and M. K. Hadj-Kali, Physicochemical properties of piperidinium, ammonium, pyrrolidinium and morpholinium cations based ionic liquids paired with bis(trifluoromethylsulfonyl)imide anion, *Fluid Phase Equilib.*, 2016, **427**, 18–26.

48 K. Shimizu, C. E. S. Bernardes, A. Triolo and J. N. Canongia, Lopes, Nano-segregation in ionic liquids: Scorpions and vanishing chains, *Phys. Chem. Chem. Phys.*, 2013, **15**, 16256–16262.

49 D. Rauber, F. Philippi, B. Kuttich, J. Becker, T. Kraus, P. Hunt, T. Welton, R. Hempelmann and C. Kay, Curled Cation Structures Accelerate the Dynamics of Ionic Liquids, *Phys. Chem. Chem. Phys.*, 2021, **23**, 21042–21064.

50 F. Philippi, D. Rauber, B. Kuttich, T. Kraus, C. W. M. Kay, R. Hempelmann, P. A. Hunt and T. Welton, Ether functionalisation, ion conformation and the optimisation of macroscopic properties in ionic liquids, *Phys. Chem. Chem. Phys.*, 2020, **22**, 23038–23056.

51 Z. J. Chen, T. Xue and J.-M. Lee, What causes the low viscosity of ether-functionalized ionic liquids? Its dependence on the increase of free volume, *RSC Adv.*, 2012, **2**, 10564–10574.

52 P. Johansson, Electronic structure calculations on lithium battery electrolyte salts, *Phys. Chem. Chem. Phys.*, 2007, **9**, 1493–1498.

53 S. Tsuzuki, K. Hayamizu and S. Seki, Origin of the low-viscosity of [emim][$(FSO_2)_2N$] ionic liquid and its lithium salt mixture: Experimental and theoretical study of self-diffusion coefficients, conductivities, and intermolecular interactions, *J. Phys. Chem. B*, 2010, **114**, 16329–16336.

54 L. Wang, Z. Luo, H. Xu, N. Piao, Z. Chen, G. Tian and X. He, Anion effects on the solvation structure and properties of imide lithium salt-based electrolytes, *RSC Adv.*, 2019, **9**, 41837–41846.

55 H. Yoon, A. S. Best, M. Forsyth, D. R. MacFarlane and P. C. Howlett, Physical properties of high Li-ion content *N*-propyl-*N*-methylpyrrolidinium bis(fluorosulfonyl)imide based ionic liquid electrolytes, *Phys. Chem. Chem. Phys.*, 2015, **17**, 4656–4663.

56 P. M. Bayley, A. S. Best, D. R. MacFarlane and M. Forsyth, Transport properties and phase behaviour in binary and ternary ionic liquid electrolyte systems of interest in lithium batteries, *ChemPhysChem*, 2011, **12**, 823–827.

57 G. M. A. Girard, M. Hilder, H. Zhu, D. Nucciarone, K. Whitbread, S. Zavorine, M. Moser, M. Forsyth, D. R. Macfarlane and P. C. Howlett, Electrochemical and physicochemical properties of small phosphonium cation ionic liquid electrolytes with high lithium salt content, *Phys. Chem. Chem. Phys.*, 2015, **17**, 8706–8713.

58 M. D. Lingwood, Z. Zhang, B. E. Kidd, K. B. Mc Creary, J. Hou and L. A. Madsen, Unraveling the local energetics of transport in a polymer ion conductor, *Chem. Commun.*, 2013, **49**, 4283–4285.

59 S. M. Green, M. E. Ries, J. Moffat and T. Budtova, NMR and Rheological Study of Anion Size Influence on the Properties of Two Imidazolium-based Ionic Liquids, *Sci. Rep.*, 2017, **7**, 1–12.

60 K. Ueno, H. Tokuda and M. Watanabe, Ionicity in ionic liquids: correlation with ionic structure and physicochemical properties, *Phys. Chem. Chem. Phys.*, 2010, **12**, 1648.

61 M. Yoshizawa, W. Xu and C. A. Angell, Ionic Liquids by Proton Transfer: Vapor Pressure, Conductivity, and the Relevance of ΔpK_a from Aqueous Solutions, *J. Am. Chem. Soc.*, 2003, **125**, 15411–15419.

62 M. Kanakubo, H. Nanjo, T. Nishida and J. Takano, Density, viscosity, and electrical conductivity of *N*-methoxymethyl-*N*-methylpyrrolidinium bis(trifluoromethanesulfonyl)amide, *Fluid Phase Equilib.*, 2011, **302**, 10–13.

63 C. Kang, O. Hutt and J. M. Pringle, Halide-free Synthesis of New Difluoro(oxalate)borate $[DFOB]^-$-based Ionic Liquids and Organic Ionic Plastic Crystals, *ChemPhysChem*, 2022, **e202200115**, 1–12.

64 K. Hayamizu, S. Tsuzuki, S. Seki, K. Fujii, M. Suenaga and Y. Umebayashi, Studies on the translational and rotational motions of ionic liquids composed of *N*-methyl-*N*-propylpyrrolidinium (P13) cation and bis(trifluoromethanesulfonyl) amide and bis(fluorosulfonyl)amide anions and their binary systems including lithium salts, *J. Chem. Phys.*, 2010, **133**, 194505–194517.

65 Z. Li, G. D. Smith and D. Bedrov, Li^+ solvation and transport properties in ionic liquid/lithium salt mixtures: a molecular dynamics simulation study, *J. Phys. Chem. B*, 2012, **116**, 12801–12809.

66 N. Sánchez-Ramírez, B. D. Assresahegn, D. Bélanger and R. M. Torresi, A Comparison among Viscosity, Density, Conductivity, and Electrochemical Windows of *N*-*n*-Butyl-*N*-methylpyrrolidinium and Triethyl-*n*-pentylphosphonium Bis(fluorosulfonyl imide) Ionic Liquids and Their Analogues Containing Bis(trifluoromethylsulfonyl) Imide Anion, *J. Chem. Eng. Data*, 2017, **62**, 3437–3444.

67 N. Tolganbek, Y. Yerkinbekova, S. Kalybekkyzy, Z. Bakenov and A. Mentbayeva, Current state of high voltage olivine structured $LiMPO_4$ cathode materials for energy storage applications: A review, *J. Alloys Compd.*, 2021, **882**, 160774–160790.

68 K. S. Kim, S. Choi, D. Demberelnyamba, H. Lee, J. Oh, B. B. Lee and S. J. Mun, Ionic liquids based on *N*-alkyl-*N*-methylmorpholinium salts as potential electrolytes, *Chem. Commun.*, 2004, 828–829.

69 G. H. Lane, P. M. Bayley, B. R. Clare, A. S. Best, D. R. MacFarlane, M. Forsyth and A. F. Hollenkamp, Ionic liquid electrolyte for lithium metal batteries: Physical, electrochemical, and interfacial studies of *N*-methyl-*N*-butylmorpholinium bis(fluorosulfonyl)imide, *J. Phys. Chem. C*, 2010, **114**, 21775–21785.

70 A. Tsurumaki, H. Ohno, S. Panero and M. A. Navarra, Novel bis(fluorosulfonyl)imide-based and ether-functionalized ionic liquids for lithium batteries with improved cycling properties, *Electrochim. Acta*, 2019, **293**, 160–165.

71 J. D. Holbrey, W. M. Reichert and R. D. Rogers, Crystal structures of imidazolium bis(trifluoromethanesulfonyl)-imide 'ionic liquid' salts: The first organic salt with a *cis*-TFSI anion conformation, *Dalton Trans.*, 2004, 2267–2271.

72 O. Palumbo, F. Trequattrini, A. Cimini, A. Tsurumaki, M. A. Navarra and A. Paolone, Inter- and Intramolecular Interactions in Ether-Functionalized Ionic Liquids, *J. Phys. Chem. B*, 2021, **125**, 2380–2388.

73 O. Palumbo, F. Trequattrini, F. M. Vitucci, M. A. Navarra, S. Panero and A. Paolone, An infrared spectroscopy study of the conformational evolution of the Bis(trifluoromethanesulfonyl)imide ion in the liquid and in the glass state, *Adv. Condens. Matter Phys.*, 2015, **2015**, 176067–176078.

74 W. A. Henderson, M. L. Helm, D. M. Seo, P. C. Trulove, H. C. De Long and O. Borodin, Electrolyte Solvation and Ionic Association: VIII. Reassessing Raman Spectroscopic Studies of Ion Coordination for LiTFSI, *J. Electrochem. Soc.*, 2022, **169**, 060515.

75 S. Duluard, J. Grondin, J. L. Bruneel, I. Pianet, A. Grélard, G. Campet, M. H. Delville and J. C. Lassègues, Lithium solvation and diffusion in the 1-butyl-3-methylimidazolium bis(trifluoromethanesulfonyl)imide ionic liquid, *J. Raman Spectrosc.*, 2008, **39**, 627–632.

76 S. Menne, T. Vogl and A. Balducci, Lithium coordination in protic ionic liquids, *Phys. Chem. Chem. Phys.*, 2014, **16**, 5485–5489.

77 F. Chen and M. Forsyth, Elucidation of transport mechanism and enhanced alkali ion transference numbers in mixed alkali metal-organic ionic molten salts, *Phys. Chem. Chem. Phys.*, 2016, **18**, 19336–19344.